BAW-132

THERMAL AND HYDRAULIC DESIGN
OF THE CONSOLIDATED EDISON
THORIUM REACTOR

July 1960

THE BABCOCK & WILCOX COMPANY

ATOMIC ENERGY DIVISION

DISCLAIMER

This report was prepared as an account of work sponsored by an agency of the United States Government. Neither the United States Government nor any agency Thereof, nor any of their employees, makes any warranty, express or implied, or assumes any legal liability or responsibility for the accuracy, completeness, or usefulness of any information, apparatus, product, or process disclosed, or represents that its use would not infringe privately owned rights. Reference herein to any specific commercial product, process, or service by trade name, trademark, manufacturer, or otherwise does not necessarily constitute or imply its endorsement, recommendation, or favoring by the United States Government or any agency thereof. The views and opinions of authors expressed herein do not necessarily state or reflect those of the United States Government or any agency thereof.

DISCLAIMER

Portions of this document may be illegible in electronic image products. Images are produced from the best available original document.

BAW-132

THERMAL AND HYDRAULIC DESIGN
OF THE CONSOLIDATED EDISON
THORIUM REACTOR

July 1960

By
J. K. Ferrell
H. E. Flora
D. R. Hostetler
L. J. Stanek
W. M. Vannoy
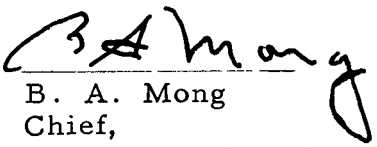
Approved by: *[signature]*
B. A. Mong
Chief,
Reactor Engineering Section

Approved by: *[signature]*
W. C. Gumprich
Manager,
Engineering Department

PREPARED FOR
THE CONSOLIDATED EDISON COMPANY OF NEW YORK
BY
THE BABCOCK & WILCOX COMPANY
ATOMIC ENERGY DIVISION
Lynchburg, Virginia

CROSS REFERENCE INDEX

This Cross Reference Index has been prepared to key the supplementary material to the information which is contained in the Hazards Summary Report dated January, 1960, Exhibit K-5 (Rev-1) filed with Amendment No. 10 to Consolidated Edison's Application for Licenses.

SECTION 2 - REACTOR DESIGN

	EXHIBIT NO.
2.1 - REACTOR DESCRIPTION	
2.1.1 Reactor Vessel and Its Internal Structure	
Consolidated Edison Thorium Reactor Reactor Vessel Internal Components Design (Report BAW-136)	K-5A1
2.1.2 Fuel Element Design	
Fuel Element Structural Design and Manufacture for the Consolidated Edison Thorium Reactor Plant (Report BAW-133)	، K-5A2
2.1.3 Control Rods, Fixed Shim Rods and Flux Depressors	
Design of the Movable and Fixed Control Components for the Consolidated Edison Thorium Reactor (Report BAW-147)	K-5A3
2.2 - THERMAL AND HYDRAULIC DESIGN	
2.2.1 General Design Data	
Thermal and Hydraulic Design of the Consolidated Edison Thorium Reactor (Report BAW-132)	K-5A4
2.2.2 Design Methods and Correlations	
Thermal and Hydraulic Design of the Consolidated Edison Thorium Reactor (Report BAW-132)	K-5A4
Irradiation Test Program for the Consolidated Edison Thorium Reactor (Report BAW-134)	K-5A5

3.1.3 Seal Water and Primary Makeup System

Supplementary Information on Plant
Design of Consolidated Edison Nuclear
Steam Generating Station   K-5A11

3.1.4 Primary Relief System

Supplementary Information on Plant
Design of Consolidated Edison Nuclear
Steam Generating Station   K-5A11

3.1.5 Primary Vent System

Supplementary Information on Plant
Design of Consolidated Edison Nuclear
Steam Generating Station   K-5A11

3.2 - SECONDARY SYSTEMS

Exhibit K-5A11 contains an introductory section
entitled, "Conventional Plant Features Contributing
to Nuclear Plant Safety." In addition, this exhibit
contains supplementary data on the following systems:

3.2.1 Steam Piping System
3.2.2 Secondary Relief System
3.2.3 Boiler Feed System
3.2.4 Boiler Blowdown System

3.3 - SUPPORTING SYSTEMS

3.3.1 Chemical Processing Systems

Supplementary Information on Plant
Design of Consolidated Edison Nuclear
Steam Generating Station   K-5A11

The Effects of Fuel Rod Fission Product
Leakage on the Consolidated Edison Thorium
Reactor Plant (Report BAW-85 Rev. 1)   K-5A13

Corrosion Product Activity Distribution
Across the Chemical Process System
for the Consolidated Edison Thorium Reactor
(Report BAW-142 Rev. 1)   K-5A14

3.3.2 Boron Addition System
3.3.3 Decay Heat Cooling System
3.3.4 Component Drain System
3.3.5 Sampling System
3.3.6 Fresh Water Cooling System
3.3.7 Electrical System

Additional data on these six supporting
systems described in the Hazards Summary
Report is contained in the report, "Supplementary
Information on Plant Design of Consolidated
Edison Nuclear Steam Generating Station"   K-5A11

Missing Pages
i-ii

CONTENTS

LIST OF TABLES

LIST OF FIGURES

ABSTRACT

The Consolidated Edison Thorium Reactor (CETR) is a thorium converter type, fueled with a mixture of thorium oxide and fully enriched oxide contained in stainless steel tubes. The active portion of the reactor core is composed of 120 box-type fuel elements. The heat generated by the fuel is transferred to the coolant (ordinary water) and transported from the reactor.

The normal flow rate of cooling water through the reactor is 52.8×10^6 lb/hr. The average water temperature at rated power (585 MWh) is 486.5 F at the reactor vessel inlet and 519 F at the reactor vessel outlet. Approximately 87% of the total flow receives heat from the fuel elements directly and the remainder of the flow is diverted to cool thermal shields, control rods, and other internals.

This report presents the thermal and hydraulic analyses, both steady state and transient, for the CETR. Methods of calculations are discussed and results of analyses are presented. Steady state analyses are included for pressure drops, flow distribution, orificing, burnout, fuel central melting, local boiling, and bulk boiling. Transient analyses are performed for several loss of forced coolant flow incidents.

Fuel melting during steady state operation and burnout cannot occur at any attainable reactor power in the CETR as designed. Bulk boiling of the coolant does not occur at any point in the core during normal steady state operation. Bulk boiling is permitted during transients because very few fuel channels are involved and the resulting effects on overall reactor performance are small. Local boiling of the coolant may occur in the reactor during normal steady state operation, and has no appreciable effect on reactor operation except a slight increase in friction pressure drop. The heat transfer characteristics of the core are actually improved.

The hydraulic transient analyses show that no risk of core damage exists for the total loss of forced coolant flow from either maximum or minimum initial flow conditions.

I. INTRODUCTION

A. REACTOR DESIGN DATA

The principal thermodynamic, hydraulic, and mechanical design data for the CETR core are summarized in Table I.

B. LIMITATIONS ON PERFORMANCE

Design limits for the performance of the CETR core are based on evaluation of the effects of thermal phenomena on the continuous operation of the reactor at rated power. These phenomena are burnout, fuel central melting, bulk boiling and local boiling. Cladding surface temperature is inherently limited by the mechanisms of bulk and local boiling.

The most serious of these design limitations is imposed by burnout (the condition resulting from a transition from nucleate to film boiling). The resulting increase in resistance to heat transfer can cause a rise in surface temperature and, under extreme conditions, can result in fuel element failure

The CETR is designed to prevent burnout at any attainable reactor power. The maximum attainable reactor power is limited to 760 MWh (130% rated power) by safety devices. It is also designed so oxide fuel melting cannot occur at any attainable reactor power during steady state operation.

The CETR is designed so bulk boiling of the coolant will not occur at any point in the core during normal steady state operation. Bulk boiling is allowed during rapid transients since very few fuel channels are involved and the resulting effects on overall reactor performance are small.

Local boiling may occur during normal steady state operation. This phenomenon has no appreciable effect on reactor operation except for a slight increase in friction pressure drop. The heat transfer characteristics of the core are actually improved.

C. POWER PEAKING FACTORS

Nonuniform power distribution is calculated using a maximum-to-average power peaking factor composed of two separate factors.

1. The radial factor is the product of the gross shaping of the power distribution in the radial direction as determined by control rod patterns

TABLE I

REACTOR DESIGN AND PERFORMANCE CHARACTERISTICS

A. **Core Materials**

Fuel	ThO_2-UO_2 mixture
Cladding	304 stainless steel, boron modified
Transition pieces	304 stainless steel
Springs	Inconel-X
Can	Zircaloy-2
Ferrules	304 stainless steel
Control rods	Hafnium
Follower rods	Zircaloy-2
Fixed shim rods	304 stainless steel, boron modified
Fixed filler rods	Zircaloy-2
Flux depressor plates	304 stainless steel

B. **Geometry**

Fuel rod OD	0 304 inches
Clad thickness	0.0205 inches
Fuel pellet diameter	0 260 inches
Fuel pellet length/diameter ratio	3
Fuel rod pitch (square)	0.374 inches
Number of fuel rods per element	195
Active fuel length per rod (cold)	98.5 inches
Ferrule OD	0 225 inches
Ferrule ID	0.189 inches
Ferrule length	0 750 inches
Number of ferrule planes	12
Element size	5.711 inches square
Element pitch	6.3225 inches
Can thickness	0.155 inches
Number of elements per core	120
Control rod pitch	12.645 inches
Control rod blade width	10.00 inches
Control rod blade thickness	0.300 inches

TABLE I (Cont'd)

REACTOR DESIGN AND PERFORMANCE CHARACTERISTICS

	Number of control rods	21
	Fixed shim blade width	10.0 inches
	Fixed shim blade thickness	0.125 inches
	Maximum number of fixed shims	24
	Maximum core diameter	84.34 inches
C.	Fluid Flow	
	Total reactor flow	52.8×10^6 lbs/hr
	Leakage flow	7.1×10^6 lbs/hr
	Velocity (inside elements)	21.5 ft/sec
	Total area inside element	29.0 inches^2/element
	Flow area (effective)	14.8 inches^2/element
	Flow area in ferrule region	12.5 inches^2/element
	Equivalent diameter for pressure drop (unit cell)	0.0237 ft
	Pressure drop (grid plate to grid plate)	43.8 psi
	Pressure drop (fuel region)	33.1 psi
	Operating pressure	1485 psig
D.	Heat Transfer	
	Reactor power	585 MWh
	Average heat flux (at 585 MWh)	128,000 Btu/hr-ft^2
	Heat transfer coefficient	9,100 Btu/hr-ft^2 °F
	Heat transfer area	15,600 ft^2
	Reactor inlet temperature (at 585 MWh)	486.5 F
	Average reactor coolant temperature rise (at 585 MWh)	32.5 F
E.	General	
	Equivalent core diameter	77.7 inches (197.3 cm)
	Total core volume (98.5 inches-length)	273.4 cu ft (7740 liters)

and variation of fuel concentration over comparatively large volumes of the core, and of the highly localized peaking which occurs in fuel rods located near large heterogeneous water areas or regions of low neutron absorption.

2. The axial factor is a measure of the variation in power along the axis of the channel from inlet to outlet of the channel, determined by the distance a group of control rods is withdrawn from the bottom of the core.

All power peaking factors are obtained from physics calculations[27], and are supported by results from critical experiments and hot exponential experiments. Since the peaking factors used in design calculations are greater than those actually calculated or measured, the results are conservative. The maximum peaking factors used for CETR design are: radial, $(\phi^*/\overline{\phi})_R = 2.2$; and axial, $(\phi^*/\overline{\phi})_A = 1.9$. The total peaking factor is the product of the individual factors, and is 4.2 for CETR. The relationship between peak power and average power is given by the following equation:

$$q'''(max) = (\phi^*/\overline{\phi})_R \ (\phi^*/\overline{\phi})_A \ q''' \ (avg) \qquad (1)$$

Symbols are defined in Table VII.

D. HOT CHANNEL FACTORS

A complete core thermal analysis includes analyses of the hot, nominal, and average channels. The maximum adverse effects of manufacturing tolerances (variations in both geometrical dimensions and physical properties) and the maximum radial power peak are combined for the analysis of a hot channel. In the analysis of a nominal channel the maximum radial power peak only is considered. Neither the adverse effects of manufacturing tolerances nor the radial power peak is considered in the analysis of an average channel.

The manufacturing tolerances are described by hot channel factors for purposes of calculation. Two types of hot channel factors are used: subfactors and overall factors. Hot channel subfactors account for the deviation from the norm of a single variable. The overall hot channel factors are products of individual subfactors. The hot channel factors used in the CETR core analyses are defined in Tables II and III.

- 4 -

The numerical values of the four overall hot channel factors for the CETR are:

$$F_{q''} = 1.035$$
$$F_{q'} = 1.034$$
$$F_\theta = 1.109$$
$$F_{\Delta T} = 1.074 .$$

These values are determined by applying the worst possible combination of manufacturing tolerances to the same channel and the final result is obviously conservative. The factors are applied to the calculations for burnout, fuel central melting, local boiling, and bulk boiling; and their specific application is discussed in following sections.

TABLE II

OVERALL HOT CHANNEL FACTORS

$$F_{q''} = (f_{FD})\,(f_\xi)\,(f_\rho)\,(f_\psi)\,(f_{Dq''})\,(f_e)$$

$$F_{q'} = F_{q''}\,/\,(f_{Dq''})\,(f_e)$$

$$F_{\Delta T} = (f'_{FD})\,(f'_\xi)\,(f'_\rho)\,(f'_\psi)\,(f'_e)\,(f_{DW})\,(f_{PW})\,(f_{BW})$$

$$F_\theta = (f_{FD})\,(f_\xi)\,(f_\rho)\,(f_\psi)\,(f_{Dq''})\,(f_e)\,(f_{Dh})\,(f_{Ph})\,(f_{Bh})$$

$F_{q''}$ — Hot channel factor on heat flux, ratio of maximum heat to nominal heat flux.

$F_{q'}$ — Hot channel factor on lineal heat rate, ratio of maximum heat rate to nominal heat rate.

$F_{\Delta T}$ — Hot channel factor on coolant temperature rise, ratio of maximum to nominal coolant temperature rise.

F_θ — Hot channel factor on film temperature rise, ratio of maximum to nominal film temperature rise.

TABLE III

HOT CHANNEL SUBFACTORS

f_{FD} --   Effect of variation of fuel diameter at a point.

f'_{FD} --   Effect of variation of fuel diameter over active fuel length.

f_{ξ} --   Effect of variation of fuel enrichment at a point.

f'_{ξ} --   Effect of variation of fuel enrichment over active fuel length.

f_{ρ} --   Effect of variation of fuel density at a point.

f'_{ρ} --   Effect of variation of fuel density over active fuel length.

f_{DW} --   Effect of variation in rod diameter on coolant.

f_{Dh} --   Effect of variation in rod diameter on film coefficient.

$f_{Dq''}$ --   Effect of variation in rod diameter on heat flux.

f_{ψ} --   Effect of variation of fuel mixing at a point.

f'_{ψ} --   Effect of variation of fuel mixing over active fuel length.

f_{e} --   Effect of variation of fuel eccentricity at a point.

f'_{e} --   Effect of variation of fuel eccentricity over active length.

f_{Ph} --   Effect of variation in rod pitch on film coefficient.

f_{Bh} --   Effect of variation in rod bow on film coefficient.

f_{PW} --   Effect of variation in rod pitch on coolant.

f_{BW} --   Effect of variation in rod bow on coolant.

II. STEADY STATE ANALYSES

A. HYDRAULIC DESIGN

1. Introduction

Knowledge of the hydraulic characteristics of a reactor system is required for design of the system. The effects of channel geometry, fluid inlet conditions, flow rate, heat input, and power distribution on pressure drop and core flow distribution must be accurately determined. Theoretical methods of analysis and experimental correlations are presented, and the reliability of the methods is demonstrated.

2. Pressure Drop

Calculation of pressure drops within the reactor system is based on standard methods derived from theory and from the results of experiments. Methods are developed for analysis of single phase flow, with and without local boiling; and for analysis of two phase flow.

All pressure drop calculations are based on the following equation:

$$\frac{G^2 dv}{g} + \frac{vG\, dG}{g} + \rho dZ + dP + \rho \delta F = 0 \qquad (2)$$

if the equation is integrated over a short enough length with a uniform flow area, average values of velocity and density may be used and the equation becomes:

$$\Delta P = P_2 - P_1 = -\bar{\rho}\,(Z_2 - Z_1) - \frac{G^2}{g}\,(v_2 - v_1) - \bar{\rho}\,F \qquad (3)$$

where the Δ notation indicates downstream values minus upstream values.

The pressure drop equation (3) can be divided into several components.

Friction pressure drop, $\Delta P_f = -\bar{\rho}\,F$ $\qquad (4)$

Acceleration pressure drop, $\Delta P_a = -\dfrac{G^2}{g}\,(v_2 - v_1)$ $\;(5)$

Head loss, $\Delta P_h = -\bar{\rho}\,(Z_2 - Z_1)$ $\qquad (6)$

A change in flow area requires an additional term which is, for expansion,

$$\Delta P_e = + \bar{\rho} \frac{V_1^2}{2g} \left[1 - \sigma^2 - K_e \right] , \qquad (7)$$

and for contraction,

$$\Delta P_c = - \bar{\rho} \frac{V_2^2}{2g} \left[1 - \sigma^2 - K_c \right] . \qquad (8)$$

The two preceding equations were developed by Kays and London[1]. In both cases σ is the ratio of the smaller to the larger flow area ($\sigma < 1$).

As previously stated, the fluid equation is integrated over a small length of channel and an incremental method of solution is used. The digital computer program used to calculate pressure drops is based on this incremental method to provide for variable heating rate and flow area.

    a.   Single Phase Flow

For single phase flow, the friction pressure drop takes the form

$$\Delta P_f = - \bar{\rho} F = - \frac{fL}{D_e} \bar{\rho} \frac{V^2}{2g} \qquad (9)$$

where f is the Moody friction factor[2]. The equation best fitting the Moody curves for machine use is

$$f = \left\{ 2 \log_{10} \left[\frac{\epsilon / D_e}{3.715} - \frac{5.028}{R_e} \log_{10} \left(\frac{\epsilon / D_e}{3.175} + \frac{16.76}{R_e} \right) \right] \right\}^{-2} . \qquad (10)$$

Calculations have demonstrated that equation 10 fits the Moody curves within about 1% for turbulent flow.

Acceleration and head losses are calculated with equations 5 and 6 respectively.

    b.   Single Phase Flow With Local Boiling

Local boiling increases pressure drop due to friction. Of the few available correlations of experimental data, the one proposed by Westinghouse Atomic Power Division (WAPD)[3] appears to be the best. The following equations represent the WAPD correlation:

$$\frac{f_{lb}}{f} = \left[1 - 0.0025 \, \Delta T^* \right] \left[1 + 0.76 \frac{(10^6)}{G}^{2/3} \psi \right] \qquad (11)$$

- 8 -

$$h = 0.23 \frac{K}{D_e} (R_e)^{0.8} (Pr)^{1/3} \tag{12}$$

$$\Delta T_f = q''/C_h h \tag{13}$$

$$\Delta T_{J\&L} = T_{sat} + \frac{60(q''/10^6)^{0.25}}{e^{P/900}} - T_B \tag{14}$$

$$\Delta T^* = \Delta T_f, \quad \Delta T_{J\&L} > \Delta T_f \tag{15}$$

$$\Delta T^* = \Delta T_{J\&L}, \quad \Delta T_{J\&L} \leq \Delta T_f \tag{16}$$

$$\Psi = 1 - \frac{\Delta T^*}{\Delta T_f}. \tag{17}$$

A combination of equations 12 through 16 is used to calculate the point at which local boiling begins. The friction pressure drop for local boiling therefore becomes:

$$\Delta P_f = - \frac{f_{lb}}{f} \frac{fL}{D_e} \bar{\rho} \frac{V^2}{2g} \tag{18}$$

The pressure drops due to acceleration, fluid head, and expansion and contraction are unaffected since local boiling has little effect on fluid density. Egen and Dinges[4], and Reynolds[5], have produced experimental evidence substantiating this assumption to within a few degrees of the saturation temperature.

    c.   Two Phase Flow

        Two phase flow with bulk boiling begins when the fluid temperature equals the saturation temperature. In two phase flow the acceleration and head pressure drops both depend on fluid density and are strongly dependent upon the volume fraction of steam in the channel. Generally, the steam and water do not flow at the same velocity; however, if the relative velocities of the steam and water are known, it is possible to calculate the steam volume fraction and hence the mixture density as a function of position.

        The relative velocity of the system is defined as $V_R = V_g - V_f$, where V_g and V_f are the average steam and water velocities respectively. The slip ratio is defined as V_g/V_f. These

definitions assume an average velocity can be assigned to each phase, and no pressure gradient normal to the direction of flow exists.

A weight balance at any point in the channel gives expressions relating steam quality, steam volume fractions, and slip ratio. These expressions are

$$X = \frac{1}{1 + \frac{V_f}{V_g} \frac{\rho_f}{\rho_g} (\frac{1}{\alpha} - 1)} ,$$ (19)

or

$$\alpha = \frac{1}{1 + \frac{V_g}{V_f} \frac{\rho_g}{\rho_f} (\frac{1}{X} - 1)} .$$ (20)

A relative velocity correlation based on experimental data of Behringer[6] (Figure 1) is used for slip data. Experimental results from ANL[7] are slightly higher than the values obtained from the correlation. Calculated pressure drops using different values of slop ratio compare favorably with the experimental data of Jakob[8]. For purposes of machine calculations the following equation has been fitted to Figure 1,

$$V_R = a + b\alpha^c$$ (21)

V_R and α are obtained by the iterative solution of equations 20 and 21. Steam quality is calculated with a heat balance.

Two phase friction pressure drops are calculated using the method of Martinelli and Nelson[9] modified by a correlation for the effect of mass velocity derived at WAPD[3]. The WAPD correction is applied as a multiplier and is suitable for an incremental pressure drop calculation. The Martinelli and Nelson curves have been fitted by the following equation:

$$\left(\frac{dP}{dL}\right)_{TPF} / \left(\frac{dP}{dL}\right)_o = \sum_{n=0}^{5} \theta_n X^n$$ (22)

where the θ_n are functions of pressure. The WAPD correction factor is

$$C = 1 + A \sqrt{X} + BX$$ (23)

where

$$A = \sum_{n=0}^{8} A_n \, (G/10^6)^n \qquad (24)$$

$$B = \sum_{n=0}^{8} B_n \, (G/10^6)^n . \qquad (25)$$

The constants in equations 24 and 25 are also pressure dependent. The corrected friction multiplier therefore becomes

$$\frac{f_{TPF}}{f_o} = \left[\sum_{n=0}^{5} \theta_n X^n \right] \left[1 + A\sqrt{X} + BX \right] , \qquad (26)$$

and the friction loss is

$$\Delta P_f = -\frac{f_{TPF}}{f_o} \frac{f_o L}{D_e} \rho_f \frac{V_f^2}{2g} . \qquad (27)$$

In this equation, f_o is the Moody friction factor with the whole channel filled with saturated water.

The acceleration pressure drop for two phase flow takes the form:

$$\Delta P_a = -\frac{G^2}{g} \left[\frac{(1-X)_2^2}{(1-\alpha)_2} + \frac{X_2^2}{\alpha_2} \frac{\rho_f}{\rho_g} - \frac{(1-X)_1^2}{(1-\alpha)_1} - \frac{X_1^2}{\alpha_1} \frac{\rho_f}{\rho_g} \right] \frac{1}{\rho_f} \qquad (28)$$

where the subscripts 2 and 1 represent the upstream and downstream limits of the increment respectively.

Fluid head for incremental pressure drop calculations is obtained from the equation

$$\Delta P_h = -L \left[\rho_f + \frac{\alpha_1 + \alpha_2}{2} \rho_g - \frac{\alpha_1 + \alpha_2}{2} \rho_f \right] . \qquad (29)$$

It is assumed the average density in the increment is the linear average of the terminal values.

Because of the scarcity of experimental data on expansion and contraction during two phase flow, a theoretical method of calculation similar to that used for two phase friction has been devised. The expansion and contraction losses are calculated for a single phase of saturated

fluid and corrected by a multiplier. The resulting equations are

$$\Delta P_c = - \bar{\rho} \; \frac{V_2^2}{2g} \left[1 - \sigma^2 \right] \; - I \, K_c \; \rho_f \; \frac{V_{f2}^2}{2g} , \tag{30}$$

and

$$\Delta P_e = \bar{\rho} \; \frac{V_1^2}{2g} \left[1 - \sigma^2 \right] \; - I \, K_e \; \rho_f \; \frac{V_{f1}^2}{2g} \tag{31}$$

where

$$I = \left[1 + X (\sqrt{V_g / V_f} - 1) \right]^2 . \tag{32}$$

The preceding equations assume the slip ratio does not change with changes in flow area and the pressure changes are too small to affect X and a.

Orifice data for two phase flow obtained by Hoopes[10], show good agreement with the above equations.

Weiss[11] reported results of pressure drop experiments covering nonboiling, local boiling, and bulk boiling within a vertical, uniformly heated tube of uniform cross section. Pressure drops calculated by the methods described are within 11% of these experimental results and the average deviation is approximately 4%. The results of one of the experiments of Weiss are plotted with calculated pressure drops in Figure 2.

Pressure drops for single phase flow were measured experimentally in a full scale model of a CETR fuel element at the B&W Research Center. The only significant deviations from accepted correlations were the contraction coefficient at the inlet transition piece and the combined contraction and expansion coefficient at the ferrule planes. Experimental values for these were determined to be 0.54 and 0.32 respectively. Using these experimental values, the calculated pressure drop for the test element agreed with the measured pressure drop to within about 2%.

The results of pressure drop calculations at rated power are given in Table I.

3. Flow Distribution

The distribution of coolant flow within a reactor core is calculated using the theory of parallel flow. This theory states that parallel channels connecting common plenum chambers all have the same pressure drop, and that flow in the various channels adjusts itself to produce the required pressure drop.

The complex geometry of a fuel bundle complicates calculations of flow distribution. For simplification, each unit cell in a fuel bundle is assumed to be a separate flow channel in parallel with all other channels in the bundle. The flow channels are assumed to be isolated from each other without fluid mixing, either from crossflow or from turbulence created by ferrules. Comparisons with calculations where crossflow is allowed and the pressure drop is balanced at all points along the channel are inconclusive; however, there are indications that isolated channel calculations are conservative.

Leakage flow through the control rod channels, between cans, and through the thermal shields is controlled by orifices. The method for sizing these orifices is described later.

A flow distribution analysis necessarily involves a trial and error solution. Briefly, the method is as follows. A plot of pressure drop versus flow rate is made for each different type of fuel channel. (This information is obtained from the computer program previously mentioned.) Any chosen pressure drop fixes a certain flow for each type of channel and with the number of each type of channel known, it is possible to obtain a total core flow for the chosen pressure drop.

Experimental results from a 1/24 scale flow model of the CETR core indicate a flow distribution factor of 1.038 to account for maldistribution of flow between fuel elements because of flow conditions in the lower plenum. This factor is twice the measured standard deviation from the average channel. Tests have also been performed on the distribution of flow within a fuel bundle. Flow in the bundle is uniformly distributed within the accuracy of the experimental data.

Because of the absence of boiling at rated power, flow distribution in the core is uniform except for the factor discussed above. Flow distribution for operation in excess of rated power is discussed in Section II B.

4. Orificing

Orifices control the flow rates for cooling the vessel wall, thermal shields, control rods, and other internal components of the reactor. The orifices are located and sized so the coolant flow rates are sufficient to prevent excessive thermal stresses in the reactor components without starving the fuel elements. The location of the orifices is described in Table IV and shown in Figures 3 and 4. Calculations to determine orifice diameters are

summarized in Table IV. There is an admitted uncertainty in the orifice calculations, and the design method is proportionately conservative.

The following equations are solved for the orifice flow area or diameter:

$$\Delta P = \frac{1}{K_o^2} \frac{V^2}{2g} \frac{\rho}{144} \qquad (33)$$

and

$$V = \frac{W}{\rho A}, \qquad (34)$$

where K_o is the discharge coefficient including the velocity of approach. The methods used to determine design values of the discharge coefficient, pressure drop, and flow rate for each orifice are described in the following sections.

    a. Orifice Coefficients

        Discharge coefficients were measured experimentally for all orifices except those in thin plates. Because of abnormal flow conditions, flow tests were made in mock-ups of the reactor flow channels for the following orifice types: control rod nozzle seal orifices, lower grid plate orifices at the rib intersections, and thermal shield orifices. The flow conditions for other orifice types approximate those for standard pipe orifice measurements. The measured discharge coefficients for short-tube, squarepedge orifices are in good agreement with the values reported in Kent's Mechanical Engineer's Handbook[12]. Precise discharge coefficients for standard orifices in thin plates are given in Fluid Meters[13]. The value and source of each discharge coefficient used in design calculations are shown in Table IV.

    b. Orifice Pressure Drops

        The orifice pressure drops are set to give a minimum differential pressure across the fuel can wall. If the total orifice flow rate is 25% less than the design value (with a resultant increase in the flow rate through the fuel elements), the differential pressure across the fuel can will not exceed the maximum design value of 18 psi. The pressure drop across each orifice is given in Table IV and is shown on the pressure map in Figure 3.

    c. Orifice Flow Rates

        The flow rates for the annuli between thermal shields, the channels between fuel elements, and the hold-down columns are controlled by orifices above or below the channels. The orifice flow rates are set to

prevent excessive thermal stresses in the internal components as a result of thermal gradients and differential thermal expansion. For temperature distribution calculations, the heat generation rates include a safety factor of 1.5 for the thermal shields and 1.25 for the core internals. The flow rates are sufficient to prevent local boiling on the surface of any internal component and provide equal pressure drops for all parallel channels between fuel elements. Maldistribution of flow between parallel channels will not result from unequal channel flow resistance or from increased local boiling pressure drop. A summary of the reactor flow distribution is given in Table V, and orifice flow rates are given in Table IV.

The effect of seal leakage on the orifice flow rates was calculated for the orifice seal ring, the thermal shield (piston ring) seal, the control rod nozzle seals, and the seals between mating surfaces of components. In each case, the seal geometry can be approximated by an annulus of by parallel plates with fine clearance. The Nootbar and Kinter[14] correlations for friction factor in flow passages with fine clearance are used in design calculations

$$\frac{f}{4} = \frac{21.6}{R_e} \quad \text{For laminar flow range,} \tag{35}$$

and

$$\frac{f}{4} = \frac{0.054}{(R_e)^{0.2}} \quad \text{For turbulent flow range.} \tag{36}$$

Entrance and exit loss coefficients from Kays and London[1] are used for square-edge annular orifices and parallel plates. For round-edge annular orifices, the sum of the entrance and exit loss coefficients is 1.01 as recommended by Bell and Bergelin[15]. Experimental work by Schneckenberg[16] and by Tao and Danovan[17] shows that the flow rate through a fully eccentric annular orifice is about 1.3 times the flow rate through a concentric annulus. Leakage calculations made by dividing the seal ring into $30°$ sectors confirmed this flow increase for the eccentric annulus. As-built dimensions, corrected to operating temperature, are used in the seal calculations. The results show that the leakage flow rates are small for all seals except the orifice seal ring. The leakage flow rate for the piston ring seal was verified by experiment. The maximum leakage was about 4.5 lbs/sec for $70°F$ water and a 50 psi pressure differential.

The flow through the orifice seal ring is a major portion of the flow leaving the core region and will vary with the eccentricity of the seal annulus. There is no means of centering the upper grid assembly in the orifice seal ring, and the annulus will be at least partially eccentric. The orifice seal ring is assumed fully eccentric for design calculations to reduce the possibility of diverting too much flow from the fuel elements.

Design calculations are based on a total flow rate through the fuel elements of 45.7×10^6 lbs/hr and a flow rate outside the fuel elements of 5.5×10^6 lbs/hr. A flow rate of 1.6×10^6 lbs/hr, 29% of the design orifice flow, is allowed for uncertainty in orifice calculations and miscellaneous leakage.

B.   THERMAL DESIGN

1.   Introduction

The primary function of a reactor is to produce heat, and a complete knowledge of thermal analysis procedures is necessary to satisfactorily design such a plant. The thermal design procedures included in this section predict burnout, fuel central melting, local boiling and bulk boiling conditions.

2.   Burnout

Burnout is the most severe limitation controlling the design of a water cooled reactor. It is defined for the purposes of this analysis as the condition when nucleate boiling on a heated surface ends and film boiling begins. This condition can be produced by various combinations of heat flux, coolant flow rate, temperature, and pressure. When a film of steam is suddenly formed on the heated fuel cladding surface, resistance to heat transfer increases rapidly. The clad surface temperature increases, and melting of the cladding is possible.

The burnout correlation used for the CETR design was determined by fitting an equation to available burnout data including recent data from Argonne National Laboratory and from The Babcock & Wilcox Company's Research Center. The form of the correlation is the same as that developed by WAPD[18]. Additional data have been included to substantiate the validity of the correlation.

The equation used expresses the burnout heat flux as a function of (a) the coolant enthalpy at the burnout point, (b) the coolant mass velocity, (c) the length of heated channel, and (d) the hydraulic equivalent diameter of that channel. The curve which best fits the above described data is reduced by a factor of 1.54 to account for scatter of the data. This curve is used in

TABLE IV

SUMMARY OF CETR ORIFICE CALCULATIONS

Number of Orifices	Orifice Location (See Fig. 3)	Description of Orifice	Total Flow, lb/sec	Water Temp, °F	Orifice ΔP, psi	Orifice Diameter, inches	Orifice Discharge Coefficient
60	(1)	Orifice for flow between innermost and second thermal shields	137	510	50 6	0 328	0 79**
30	(2)	Orifice for flow between second and third thermal shields	49	510	50 6	0 266	0 81**
9	(3)	Orifice for flow between third thermal shield and vessel wall	21	510	50 6	0 328	0 81**
		TOTAL FLOW BETWEEN THERMAL SHIELDS	207				
28		Orifice for flow through holddown column (at top of main tube)	86	510	44.0	0 406	0 77**
112		Orifice for flow outside holddown column (in wall of main tube near bottom)	156	486 5	24 0	0 406	0 60[13] (+ Bend Loss)
		TOTAL HOLD-DOWN COLUMN FLOW	242				
4	(4)	Orifice for flow between core shroud and inner thermal shield-position D-Figure 4	40	490	26 0	0 813	0 80***
8	(5)	Orifice for flow between core shroud and inner thermal shield-position E-Figure 4	66	490	26 0	0 734	0 80***
8	(6)	Orifice for flow between core shroud and inner thermal shield-position F-Figure 4	44	490	26 0	0 594	0 80***
		TOTAL FLOW BETWEEN CORE SHROUD AND FIRST SHIELD	150				
84	(7)	Orifice for control rod nozzle seal 4 each control rod drive shaft	324	486 5	26 0	0.500	0 80**
42	(8)	Orifice for control rod nozzle thermal sleeve heating water 2 each drive shaft	40	486 5	26 0	0 25	0 80***
24	(9)	Orifice at rib intersection lower grid plate-position A-Figure 4	115	490	24 0	0 563	0 82**
12	(10)	Orifice at rib intersection lower grid plate-position B-Figure 4	133	490	24 0	0 859	0 82**
16	(11)	Orifice in lower grid plate-position C-Figure 4	320	490	24 0	1 172	0 79***
		TOTAL FLOW BETWEEN FUEL ELEMENTS	932				
		TOTAL FLOW INTO CORE REGION	1238				
16	(12)	Orifice in upper grid plate-position C-Figure 4	168	520	20.0	0 875	0.80***
21	(13)	Orifice for control rod guide tube-thin plate	460	520	20 0	1 469	0 61[13]
	(14)	Orifice seal ring-eccentric plus seating surface leakage	610	520			
		TOTAL FLOW OUT OF CORE REGION	1238				
		TOTAL ORIFICE FLOW	1531				

* - Including Velocity of Approach

** - From Flow Test Mockup of Reactor Flow Channel

*** - From Flow Test For Short-Tube Orifices in Pipes

TABLE V

SUMMARY OF REACTOR FLOW DISTRIBUTION

REGION	FLOW RATE	
	lbs/sec	lbs/hr x 10^6
Fuel elements	12,694.4	45.70
Between fuel elements		
Control rod channels	350.0	1.26
Fixed shim channels	114.8	0.41
Other channels between elements	467.6	1.68
Between innermost thermal shield and core shroud	150.0	0.54
Between thermal shields	207.0	0.75
Holddown columns	242.2	0.87
Allowance for uncertainty in orifice flow and miscellaneous leakage	444.4	1.60
TOTAL REACTOR FLOW	14,670.4	52.8

determining the maximum permissible heat flux.

The maximum permissible heat flux is also reduced by 20 per cent to account for uncertainties, and the resulting correlation is used as the maximum design heat flux curve. Results of tests made by the AEC Bettis Laboratory indicate that this design curve is conservative. Four bundles of nine tubes were tested to the point of physical burnout. The heat fluxes at burnout were at least 65 per cent above the design curve. A plot of several heat flux correlations is given in Figure 5 for purposes of comparison. The equation developed for the maximum permissible heat flux is:

$$\frac{q''_{B.O.}}{10^6} = \frac{0.182 \left(1 + \frac{G}{10^7}\right)^2}{F_s \left(\frac{h_i}{10^3}\right)^{2.5} e^{0.0012 \frac{X_i - X_e}{D_e}}}. \tag{37}$$

The heat flux calculated with the preceding equation (with $F_s = 1.2$) is defined as the maximum design heat flux. The burnout heat flux analysis is a combination of several of the calculation methods previously mentioned. The first step is to determine the pressure drop in the core at rated flow. This is found by computing the pressure drop for a fuel element at rated power and flow rate with all hot channel and peaking factors equal to unity. The pressure drop for the average channel is the same as that of the average element, and of the core. All peaking and hot channel factors including that for maldistribution of flow are then applied to the hot channel, and a hot channel flow rate is computed. This procedure is repeated for a series of power levels.

With the coolant conditions along the hot channel as a function of power level, the maximum design heat flux is computed and compared with the actual surface heat flux in that channel. This procedure is repeated for various power levels until the surface heat flux and the maximum design heat flux become just equal at some point in the hot channel. This power level is defined as the maximum safe reactor power level.

Figure 6 illustrates the results of the burnout heat flux analysis for rated power operation (585 MWh). A radial peaking factor of 2.2 is assumed. This is a value slightly higher than the highest value calculated in the CETR control rod programming studies. A cosine axial power distribution with a calculated peak-to-average ratio of 1.5 is assumed. The

analysis is performed for the hot channel, and the hot channel factors listed in Section I D are used. Even with all burnout safety factors included, the minimum ratio of burnout heat flux to actual heat flux is 2.48.

The surface heat flux in the hot channel increases as the power level is increased above rated power. In steady state, the coolant inlet temperature also increases and causes a change in the coolant flow rate and properties in the hot channel. As a result the maximum design heat flux decreases. Figure 7 illustrates the results of the thermal analysis of the hot channel (all hot channel factors applied) for operation at 837 MW (143% rated power). Since the surface heat flux and maximum design heat flux curves are just tangent, this power level is the maximum safe reactor power level. Moreover, experimental evidence previously cited indicates that in any event the surface heat flux may exceed the maximum design heat flux by as much as 20% without damage.

The results of the flow distribution calculation for the case illustrated in Figure 7 show a flow reduction in the hot channel of 23% due to the effects of boiling in that channel. The exit quality in the hot channel is 0.164.

The control rod programming studies have also indicated axial peaks in the bottom of the core when control rods are only partially withdrawn. The highest expected maximum to average ratio is 1.9. Since the peak is in the bottom of the core where the water sub-cooling is greatest, the higher peaking factor can be tolerated. The maximum safe reactor power level for this condition was determined to be 790 MW (135% rated power).

The two cases described are the extreme cases; all other maximum safe reactor powers for other axial power peaks are located between them.

Methods of calculating maximum design heat flux for partial flow conditions are identical to those used for normal flow calculations. The flux flow computer in the reactor control system limits the reactor power to a preset power level for each partial flow condition. These power levels are listed in Table VI in the column headed "Average Power". The maximum safe reactor power level for each partial flow condition is also shown.

TABLE VI

MAXIMUM SAFE REACTOR POWER AT PARTIAL FLOW

Case No.	No. Pumps	No. Loops	W_R (lbs/hr)	T_E $^\circ$F	Average Power, MWh	Maximum Safe Reactor Power MWh
1	7	4	49.35×10^6	482.0	502	680
2	6	4	45.58	481.0	465	630
3	6	3	42.24	484.5	431	572
4	5	4	41.38	480.5	418	570
5	5	3	37.93	482.0	371	516
6	4	4	36.96	473.0	391	527
7	4	3	33.25	480.0	324	454
8	4	2	29.50	483.5	274	396
9	3	3	28.47	473.0	290	401
10	3	2	24.58	481.0	228	333
11	2	2	19.30	473.0	190	275

3. Fuel Central Melting

The second design limit for an oxide fueled reactor is the possible effect of oxide melting. Several irradiation experiments have been performed to determine the effect of fuel melting on reactor operation. The results thus far indicate fuel central melting will not adversely affect fuel rod integrity; however, they do not allow definite conclusions for use in reactor design. The CETR is designed to prevent fuel central melting under normal operation conditions.

The most important single factor in determining fuel central temperatures is the oxide thermal conductivity since the fuel central temperature is nearly inversely proportional to it. The thermal conductivity of ThO_2 has been investigated by Kingery et.al.[19], and by the B&W Research Center. The two sets of data are in agreement. A fifth order polynominal was fitted by the least squares method to all the experimental data. The expression corrected to theoretical density is:

$$K = 7.958 - 6.0857 \times 10^{-3} T + 2.0431 \times 10^{-6} T^2$$
$$- 0.2992 \times 10^{-9} T^3 + 0.0161 \times 10^{-12} T^4 \qquad T \leq 3500 \text{ F}$$

$$K = 1.28 \text{ Btu/lb ft F.} \qquad\qquad T > 3500 \text{ F} \quad (38)$$

The thermal conductivity is assumed to be proportional to density and unaffected by irradiation.

Experimental evidence obtained at WAPD[20] and Chalk River[21] support these assumptions.

The maximum and average fuel temperatures and the power level at which fuel melting may occur are calculated on the basis of heat conduction through a cylinder made up of a clad, a gas-filled gap between clad and fuel, and a fuel pellet.

Two assumptions are made concerning the composition of the gas occupying the gap between the pellet and the clad:

(1) For irradiation times beyond 50 rated power days the gap is filled with the fission product gases, xenon and krypton (the gap conductivity being 0.01 Btu/hr-ft-F).

(2) For irradiation times up to 50 rated power days the gap is filled in with a mixture of xenon, krypton, and helium (the gap conductivity being 0.03 Btu/hr-ft-F). If a failure of the cladding should allow water to enter the gap, the conductivity would also be 0.03 Btu/hr-ft-F.

Differential thermal expansion of the cladding and fuel is based on the average temperature of each. The variation with temperature of the thermal conductivity of both the fuel and the gas is taken into account. The thermal expansion of the oxide fuel is greater than the cladding, and the oxide pellet may expand to contact the cladding. A contact coefficient defined as the thermal conductivity of the gap medium divided by the contact gap width (0.0002 inches) is used for heat transfer purposes when the pellet and clad are in contact.

Experimental verification of the foregoing methods of calculation was obtained from data for an experimental program carried out at Chalk River, Canada, with uranium dioxide pellet samples. A temperature which can be observed experimentally in the oxide is the melting temperature and the methods of calculation have been checked against those samples which exhibited some melting (determined by post-irradiation examination). The radius of fuel melting in the pellet was calculated and compared with the measured radius for a number of samples. Calculated results are conservative by between 5 and 25%.

Coolant conditions in the hot channel during power operation have only a small effect on the clad temperature as long as film boiling (burnout) does not occur. This small clad temperature change has a negligible effect

on the maximum fuel temperature because of the large temperature gradient in the fuel at high power. Fuel temperature, therefore, is dependent only on the specific lineal power in the fuel rod. The analytical procedure for determining fuel temperature predicts that the melting temperature will be reached at a specific lineal power output of 21.1 kw/ft during the first 50 days of operation (gap conductivity of 0.03 Btu/hr-ft-F). After 50 days, fuel melting will occur at 16.6 kw/ft (gap conductivity of 0.01 Btu/hr-ft-F).

After 50 days of operation, and with the maximum power peaking factors for a cosine axial power distribution (total peaking factor = 3.3), a power level of 960 MWh (165% rated power) must be attained before any fuel melting will occur in the hottest rod in the core (all peaking and appropriate hot channel factors applied). With the maximum power peak in the bottom of the core (total peaking factor = 4.2), a power level of 780 MW (133% rated power) must be attained for fuel melting to occur. Safety devices in the CETR preclude operation at these power levels; therefore, fuel melting in the CETR is prevented.

Results of central temperature calculations for the two cases discussed above are shown in Figure 8. The break in the curves occurs at the point where pellet and clad make contact.

4. Local Boiling

A subcooled fluid can boil in contact with a heated surface under certain conditions of fluid temperature, surface temperature, heat flux, and pressure. The effects on core performance are small since the volume fraction of steam is small during local boiling. The reactivity effect is negligible, and the primary effect on pressure drop is a slightly increased friction loss. Flow distribution is slightly affected by the increased friction losses.

The most important effect of local boiling is to maintain the temperature of a heated surface a few degrees above saturation temperature. Jens and Lottes[23] have fitted an equation to the experimental local boiling data.

$$\Delta T_{sat} = \frac{60 \, (q''/10^6)^{0.25}}{e^{P/900}} \tag{39}$$

where ΔT_{sat} is the temperature difference between saturation temperature and the temperature of the heated surface, and P is pressure (psi). Figure 9

shows the hot channel clad surface temperature and the bulk coolant temp-erature plotted against channel length at a power level of 632 MWh (108% rated power). The effect of local boiling on the clad surface temperature is illustrated.

5. Bulk Boiling

Steam is formed if heat is added to a fluid after the fluid bulk temperature reaches saturation temperature. The fluid temperature re-mains constant at saturation while the steam quality increases.

The temperature of a heated surface in contact with the fluid remains constant several degrees above saturation temperature and is calculated with the Jens and Lottes' correlation.

Figure 9 is plotted for the power level (632 MWh, 108% rated power) at which bulk boiling begins in the hot channel.

III. TRANSIENT ANALYSIS -
LOSS OF FORCED COOLANT FLOW

A. HYDRAULIC TRANSIENTS

1. General

Physical malfunctions may produce flow transients and reductions in reactor coolant flow. These flow transients may result from loss of electrical power to operating pumps, or from mechanical failure of a single pump.

The transient hydraulic characteristics of reactor coolant flow greatly affect the heat transfer capabilities of the reactor core. Since such interdependence exists, it is important to be able to predict the behavior of the primary system flow during a transient. An extension of the Arker-Lewis method[24] of analysis is used to predict primary system flow during hydraulic transients.

The analysis of hydraulic transients is based on the law of conservation of energy. When primary pumping power is lost or reduced, the kinetic energy of the system is dissipated by losses in the fluid and rotating machinery. It is possible to predict the rate of energy loss and the consequent reduction in flow by considering the following factors.

    (a) Inertia of the fluid

    (b) Inertia of the rotating equipment

    (c) System pressure drop

    (d) Pump head-capacity characteristics

    (e) Pump motor windage and friction

    (f) Variation of coupling between pump and fluid

    (g) Electrical braking due to trapped flux

    (h) Motor speed-torque characteristics

The summation of pressure head terms through the system must equal zero and can be expressed by the following general equation:

$$\Delta P_{KE} + \Delta P_P - \Delta P_R - \Delta P_L = 0 \qquad (40)$$

When the system is operating at a steady state condition, the developed pump head (ΔP_P) is equal to the summation of the pressure head losses $(\Delta P_R + \Delta P_L)$ and the summation of the pressure head due to kinetic energy (ΔP_{KE}) over the entire loop is equal to zero. During a flow transient the pump head decreases and the kinetic energy of the fluid is converted to a pressure head which helps overcome system pressure head losses. Each term of the above equation can be evaluated in terms of system flow parameters.

The kinetic energy of the fluid at any time during a transient is expressed as follows:

$$KE = 1/2\ MV^2 \tag{41}$$

$$\text{where} \quad M = \frac{\omega}{g} = \frac{LA\rho}{S} \quad \text{and} \quad V = \frac{W}{\rho A}. \tag{42}$$

Summing up the loop:

$$KE = 1/2\ \frac{W^2}{g\rho} \sum \frac{L}{A}. \tag{43}$$

Differentiating with respect to time:

$$\frac{\delta(KE)}{\delta t} = \frac{1}{g\rho} \sum \frac{L}{A}\ W\ \frac{\partial W}{\partial t} \tag{44}$$

Equation 44 represents the power produce by the kinetic energy in the fluid. This power divided by the quantity (cu ft / sec) produces a pressure head term

$$\Delta P_{KE} = \frac{1}{g} \sum \frac{L}{A}\ \frac{\partial W}{\partial t} \tag{45}$$

The developed pump head may be determined from the head capacity curves. If the pump speed is known, the head for a centrifugal pump may be expressed as follows:

$$\Delta P_P = \omega^2\ f_1^u\ \left(\frac{W}{j\omega}\right) \tag{46}$$

To evaluate the pump head during a transient, it is also necessary to consider the kinetic energy of the pump. Equation 46 shows ΔP_P is a function of the angular speed (ω) of the rotating parts. The kinetic energy of the fluids and the kinetic energy of the rotating components account for the entire kinetic energy of the system. It is possible to evaluate the rate of change of the pump speed by setting the summation of the kinetic energy, electrical, hydraulic, and windage torques equal to zero.

$$T_{KE} + T_E + T_H + T_W = 0. \tag{47}$$

The kinetic energy torque is defined as

$$T_{KE} = \frac{1}{g} I_P \frac{\partial \omega}{\partial t} . \tag{48}$$

The electrical torque may be written as

$$T_E = C f(\omega). \tag{49}$$

The hydraulic torque is defined as

$$T_H = \frac{W \omega f_1 \frac{W}{j\omega}}{j f_4 \frac{W}{j\omega} f_5 \omega \rho} . \tag{50}$$

The windage torque may be expressed as

$$T_W = K_\omega (\omega)^n . \tag{51}$$

The reactor pressure drop (ΔP_R) can be expressed as a parabolic function. If the full flow conditions are known for a specific reactor, the pressure drop may be written as

$$P_R = \frac{\Delta P_{RO}}{\left(W_{RO}\right)^n} (W_1 + W_2 ---- W_j)^n \tag{52}$$

The loop pressure drop (ΔP_L) is the summation of the losses in the individual components of the loop such as valves and piping. These are determined by conventional calculations and are not discussed in detail.

The general equations have been expanded, expressed in terms of the system parameters, and programmed for the Datatron Model 204 Electrodata computer. The program can handle 18 loops

in parallel and calculate the flow for various types of hydraulic transients.

A complete loss of pumping power causes a rapid reduction in primary system flow. The primary loop is arranged so natural circulation forces result from the difference in fluid density, and the system begins natural circulation at some time during the pump coastdown. This natural circulation force is present when all the pumps are in operation, but its magnitude is relatively insignificant. The pump head decreases and natural circulation force becomes more significant when a flow coastdown starts. At some point in the transient, the circulation becomes completely dependent upon density differentials. The method of calculating the natural circulation flow is presented in the following paragraph.

Natural circulation flow is density dependent, and it is necessary to analyze the loop thermodynamically during coastdown to determine temperatures at all points in the loop. This is accomplished by dividing the loop into finite flow sections and making an energy balance for each of these sections.

$$
\begin{array}{c}
+Q \\
\downarrow \\
\boxed{\begin{array}{ccc} W_y & \text{Vol.}_y & \rho_y \\ h_y & T_y & m_y \end{array}} \\
\downarrow \\
-Q
\end{array}
\qquad
\begin{array}{l} W_z \\ T_z \end{array}
\quad h_z
\qquad (53)
$$

$h_x \quad W_x \rightarrow \quad \quad \rightarrow W_z \quad h_z$

T_x
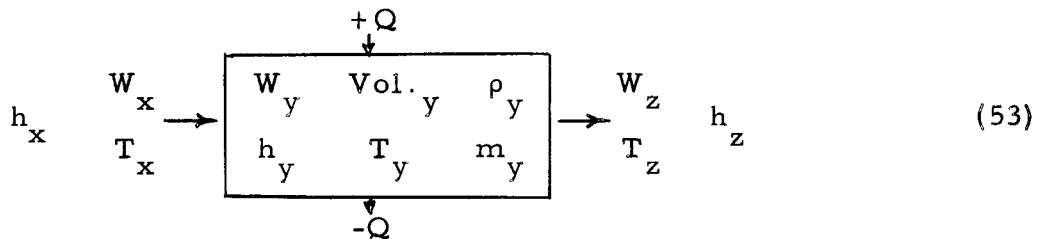
An energy balance may be written using the above diagram of a small flow section.

$$ \text{Vol.}_y \, \rho_y \, \frac{\partial h_y}{\partial t} + h_y \, \text{Vol.}_y \, \frac{\partial \rho_y}{\partial t} = Q + W_x h_x - W_z h_z \qquad (54) $$

It is possible to evaluate the energy balance in terms of T_x, T_y, Vol._y, W_x, and t; using enthalpy and density as a function of temperature with appropriate lag times. An equation is written for each section of the loop with the data generated in the pump coastdown analysis. These equations predict temperatures and densities in the loop as a function time.

A thermodynamic analysis of the pump coastdown transient indicates when the density differential attains sufficient magnitude to be of interest. After this, natural circulation begins and the flow becomes less dependent upon the conversion of kinetic energy and more dependent upon static head. The combined analysis is continued until the kinetic energy terms become insignificant and the flow may be calculated entirely by conventional natural circulation methods.

2. Results

The hydraulic transients for the CETR primary system have been analyzed by the methods described in the previous paragraphs for a partial loss of pumps and for a total loss of pumps. The flow transients for two cases of a partial loss of pumps are graphically illustrated in Figures 10 and 11. The flow transients for two cases for the total loss of pumping power are shown in Figures 12 and 13. Natural circulation forces become significant when the flow has decreased to about 30% of rated flow at 585 MWh.

Flows in the hot channel are calculated with methods exactly the same as those used for the average channel. Hot channel thermal characteristics are applied in the natural circulation calculation.

The hot channel flow is less than the average channel flow for the first seven seconds due to two phase flow pressure drop. After seven seconds, the hot channel flow becomes greater than the average channel flow as the static head increases. After eight seconds, natural circulation controls the flow rate which decreases slowly as the decay heat generation decreases.

B. THERMAL TRANSIENTS

1. General

The possibility of exceeding the steady state design limits for burnout exists during the loss of coolant flow incident. Therefore, the possibility of fuel element damage caused by the transition from nucleate to film boiling at some time during the transient has been investigated.

Temperature distribution within the fuel rod as a function of time is obtained by the numerical solution of the transient heat conduction equation.

$$k(T) \left[\frac{\partial^2 T(r,t)}{\partial r^2} + \frac{1}{r} \frac{\partial T(r,t)}{\partial r} \right] + S(r,t) = \rho C_P \frac{\partial T(r,t)}{\partial t} . \quad (55)$$

Equation 55 is solved for the three regions consisting of fuel, gap, and clad, with the boundary condition at the outside surface of the clad expressed as

$$\left[k \frac{\partial T}{\partial r} \right]_{surface} + h_{(t)} \left[T_{surface} - T_{coolant} \right] = 0 . \quad (56)$$

A numerical solution of the above equations, programmed for a digital computer, is used for the analysis   The geometrical model is similar to that used for steady state analyses. A fuel pellet is assumed to be centrally located within the cladding with a uniform gap between the two. The gap is filled with a mixture of the fission gases, xenon and krypton. As the temperatures within the fuel rod increase, the fuel pellet expands toward the cladding until a minimum gap of 0.0002 inches is reached. At this point the gap conductivity is represented by a contact coefficient which is defined as the conductivity of the gap medium divided by the minimum gap.

Inputs for the equations include heating rate within the fuel, coolant bulk temperature, coolant saturation temperature, and film heat transfer coefficient all as functions of time   The onset of local boiling is automatically calculated and the appropriate heat transfer coefficient is substituted for the input value.

Calculated results of this analysis include surface heat flux, clad surface temperature, and fuel central temperature; all as functions of time. The results for the hot channel are of greatest interest since the probability of failure is greatest in this channel.

2.   Partial Loss of Forced Coolant Flow

A detailed thermal analysis of the partial loss of flow transient was not deemed necessary because of the protection afforded by the flux flow computer. This unit establishes a scram level for each partial flow condition. Determination of the flow condition is based

on signals received from each pump motor power supply to indicate loss of that pump.

The response time of the flux flow computer is about 0.15 sec. It can be seen from Figures 10 and 11 that this time is short compared to the loop flow coastdown time for pump shutdown. Because of this quick response, the computer anticipates the flow coastdown and, if necessary, causes a scram before the coolant flow is reduced by an amount sufficient to cause core damage.

3. Total Loss of Forced Coolant Flow

The total loss of pumping power incident has been analyzed for the maximum and minimum initial flow conditions. In each case the reactor is assumed to be operating at the rated power level for that flow, and it is assumed to be scrammed as a result of the total loss of pump power.

A 350-millisecond scram delay time is assumed for the time from loss of power until control rod motion begins. (The actual scram delay time is predicted to be 150 milliseconds.) After the reactor is scrammed, natural circulation continues to cool the core and remove decay heat. Heat transfer coefficients as a function of time are calculated from flow rates given in Figures 12 and 13. Heat generation rates as functions of time are given in Figure 14.

In Figure 16, the heat flux at the hottest point in the core is compared with the maximum design heat flux as a function of time for a loss of eight pumps. The ratio of maximum design heat flux to surface heat flux is a minimum of 1.9. Figure 18 presents the same information for a loss of flow when only two pumps are operating initially. The ratio of the maximum design heat flux to surface heat flux is a minimum of 4.4. It is concluded from these analyses that loss of all forced coolant flow from either maximum or minimum initial flow conditions will not cause core damage. Since the rated operating power levels for initial flow conditions other than maximum and minimum are established on the same basis, a complete loss of forced coolant flow from any intermediate condition can also be tolerated without risk of

core damage.

A sequential loss of pumps (loss of two or three groups of pumps in series) may result in operation above the rated power level for an intermediate flow condition at the time that power to all remaining pumps is lost. The flux-flow computer provides a scram level signal for all combinations of pumps operating. If the reactor power exceeds these settings at any time during a sequential pump loss the reactor is shut down even before additional flow loss in the sequence. Thus, the worst possible circumstance is loss of all forced flow when the reactor is operating at the scram level for any flow condition. Loss of flow conditions have been analyzed with the reactor operating at the scram level to evaluate the potential danger from this cause. (Other assumptions are the same as those in the case with initial operation at rated power.) Figures 15 and 17 present the heat flux comparisons for these cases.

The maximum design heat flux correlation used to calculate the maximum design heat flux curves (equation 37) in Figures 15 through 18 is a steady state correlation and is subject to some uncertainties for transient conditions. As a check, the worst cases, Figures 15 and 17 were also analyzed assuming that film boiling $(h = 100 \text{ Btu/hr-ft}^2 \text{-F})^{25}$ starts at one second. The resulting maximum clad temperatures shown in Figures 19 and 20 are not high enough to cause damage. Since scram levels at intermediate flow conditions are established on the same basis, no damage will occur from similar circumstances at the intermediate flow condtions. and the reactor is protected from damage caused by any sequential loss of pumps.

TABLE VII

NOMENCLATURE

Symbol:

A	-	Area (sq ft)
An, Bn	-	Constants
C	-	Two-phase friction correction factor, constant
C_P	-	Heat capacity
Ch	-	Colburn equation safety factor
D_e	-	Equivalent hydraulic diameter (ft)
F	-	Energy loss due to friction
F_s	-	Safety factor in burnout correlation
G	-	Mass velocity (lb/sq ft-hr)
I	-	Multiplier for two-phase expansion and contraction
I_P	-	Rotational inertia of pump moving parts (lb-sq ft)
k	-	Coefficient of thermal conductivity (Btu/hr-ft - ^oF)
K_c	-	Contraction loss coefficient
K_D	-	Orifice discharge coefficient
K_e	-	Expansion loss coefficient
K_W	-	Constant for windage and friction torque
L	-	Length (ft)
P	-	Pressure (lb/sq ft)
Pr	-	Prandtl No.
R_e	-	Reynolds No.
S (r, t)	-	Heating rate (Btu/hr-sq ft)
T (r, t)	-	Temperature as a function of radius and time

- 33 -

TABLE VII (CONT'D)

T_B	-	Fluid bulk temperature (^{O}F)
T_E	-	Coolant inlet temperature (^{O}F)
T_H	-	Hydraulic torque (ft-lb)
T_{KE}	-	Torque due to kinetic energy of fluid (ft-lb)
T_s	-	Clad surface temperature (^{O}F)
T_{sat}	-	Coolant saturation temperature (^{O}F)
T_W	-	Windage and friction torque (ft-lb)
V	-	Velocity (ft/sec)
V_f	-	Average fluid velocity (ft/sec)
V_g	-	Average vapor velocity (ft/sec)
V_R	-	Relative steam water velocity (ft/sec)
W	-	Weight flow rate (lb/hr)
X	-	Steam quality
X_i	-	Distance along heated channel
Z	-	Height (ft)
ΔP_a	-	Pressure change due to acceleration of fluid (lb/sq ft)
ΔP_c	-	Pressure change due to contraction (lb/sq ft)
ΔP_e	-	Pressure change due to expansion (lb/sq ft)
ΔP_f	-	Pressure change due to friction (lb/sq ft)
ΔP_h	-	Pressure change due to fluid head (lb/sq ft)
ΔP_L	-	Pressure drop external to reactor (lb/sq ft)
ΔP_P	-	Developed pump pressure head (lb/sq ft)
ΔP_R	-	Pressure drop through reactor (lb/sq ft)
$\Delta T_{J\&L}$	-	Temperature drop by Jens and Lottes correlation (^{O}F)

TABLE VII (CONT'D)

a, b, c	-	Pressure dependent constants in relative velocity correlation
f	-	Moody friction factor
f_1 ( ) F_5 ( )	-	Functions
f_{1b}	-	Local boiling friction factor
f_{TPF}	-	Two-phase flow friction factor
g	-	Gravitational constant (ft/sec^2)
h	-	Film heat transfer coefficient (Btu/hr-sq ft-$^\circ$F)
h_i	-	Coolant enthalpy (Btu/lb)
j	-	Number of pumps per loop
q'''	-	Volumetric heat generation rate (Btu/cu ft-hr)
q''	-	Surface heat flux (Btu/hr-sq ft)
$q''_{B.O.}$	-	Maximum design heat flux (Btu/hr-sq ft)
r	-	Radius of fuel rod (ft)
t	-	Time
v	-	Specific volume (cu ft/lb)
α	-	Steam volume fraction
ϵ	-	Surface roughness (microinches)
n	-	Constants for calculation of f_{TPF}
ρ	-	Density (lb/cu ft)
ρ_f	-	Density of liquid phase (lb/cu ft)
ρ_g	-	Density of vapor phase (lb/cu ft)
σ	-	Ratio of flow areas
$(\phi^*/\bar{\phi})_A$	-	Axial peak to average power
$(\phi^*/\bar{\phi})_R$	-	Radial peak to average power
ω	-	Angular velocity of pump rotor (rad/sec)
$\bar{\rho}, \bar{v}, \bar{f}$, etc.	-	Indicates use of average values

BIBLIOGRAPHY

1. Kays, W. M., and London, A. L., Compact Heat Exchanger, National Press, Palo Alto, California, 1955.

2. Moody, L. F., Friction Factors for Pipe Flow, Trans A.S.M.E., Vol. 66, P. 671, 1944.

3. Sher, N. C, Estimation of Boiling and Non-Boiling Pressure Drop in Rectangular Channels at 2000 Psia, WAPD-Th-300

4. Egen, R., and Dinges, D., Vapor Formation and Behavior in Boiling Heat Transfer, BMI-1163.

5. Reynolds, J. B., Local Boiling Pressure Drop, ANL-5178, March 1954.

6 Behringer D., Velocity of Rise in Steam Bubbles in Boiler Tubes, Verein Deutscher Inginiever Forschurgscheft, 365 B, 1935.

7. Richardson, B. L., Some Problems in Horizontal Two Phase Two Component Flow, ANL 5949, 1958

8. Jakob, Max, Leppert, G., and Reynolds, J. B., Pressure Drop During Forced Circulation Boiling, Chem. Engr. Progress Symposium, Series No. 18 - Vol. 52, 1956.

9. Martinello, R. C., and Nelson, O. B., Prediction of Pressure Drop During Forced Circulation Boiling of Water, Trans. A.S.M.E., August 1948.

10. Hoopes, J. W., Jr., Flow of Steam-Water Mixtures in a Heated Annulus and Through Orifices, AIChE Journal 3 268, 1957.

11. Weiss, D. H., Pressure Drop in Two-Phase Flow, AECU-2180, October 1952.

12. Kent's Mechanical Engineer's Handbook, 12th Edition, Power. John Wiley 1954 - Table 1 Section 5-10.

13.   ASME Research Committee on Fluid Meters, <u>Fluid Meters,</u>
      5th Edition, Table 15.

14   Nootbar, R. F., Kintner, R. C., <u>Fluid Friction in Annuli</u>
      <u>of Small Clearance,</u> Proceedings of the 2nd Midwestern
      Conference on Fluid Mechanics, Ohio State Engineering
      Experiment Station Bulletin No. 149, PP 185-194, 1952.

15.   Bell, K. J., Bergelin, O. P., <u>Flow Through Annular</u>
      <u>Crifices,</u> Trans. ASME, April 1957

16.   Schneckenberg, E., <u>Der Durchfluss von Wasser Durch</u>
      <u>Konzentrische und Excentrische Zylindrische Drosselspalte</u>
      <u>mit und ohne Ringnuten,</u> Zeitschrift fur Angewandte Mathematik
      und Mechanik, Vol. II, 1931.

17.   Tao, L. N., Donovan, W. F., <u>Through Flow in Concentric</u>
      <u>and Eccentric Annuli of Fine Clearance With and Without</u>
      <u>Relative Motion of the Boundaries,</u> Trans. A.S.M.E.,
      November 1955.

18.   DeBortoli, R. A., et al, <u>Forced Convection Heat Transfer</u>
      <u>Burnout Studies for Water in Rectangular Channels and Round</u>
      <u>Tubes at Pressure above 500 psia,</u> WAPD-188, October 1958.

19.   Kingery, W. D., Francl, J. et al <u>J. Am Cer Soc. 37,</u> 1954

20,   <u>Technical Progress Report-Pressurized Water Reactor,</u>
      Period June 24 to August 23, 1959 - WAPD MRP-81.

21.   Bail, A. S. and Robertson, J. A. L, <u>UO_2 Irradiations of</u>
      <u>Short Duration,</u> AECL-806, April 1959.

22.   Lambertson et al, <u>Urania-Thoria Binary Systems,</u> ANL-4923,
      1952.

23.   Jens, W. H., and Lottes, P. A. <u>Analysis of Heat Transfer</u>
      <u>Burnout Pressure Drop and Density Data for High Pressure</u>
      <u>Water,</u> ANL-4627, May 1951.

24.   Arker, A. J., Lewis, D. G., <u>Rapid Flow Transients In</u>
      <u>Closed Loop,</u> USAEC Reactor Heat Transfer Conference,
      November 1956.

25. Mendler, O. J. Estimated Film Boiling Heat Transfer
     Coefficients, WAPD-Th-404, March 26, 1958.

26. Jacob, W. M., et al, Thermal Design Criteria for
     Pressurized Water Reactors, Nucleonics, Novermber 1958.

27. BAW 120, Rev 1, CETR Physics Design, July 1960.

FIGURES

FIG. 1: RELATIVE VELOCITY OF STEAM IN STEAM-WATER MIXTURE
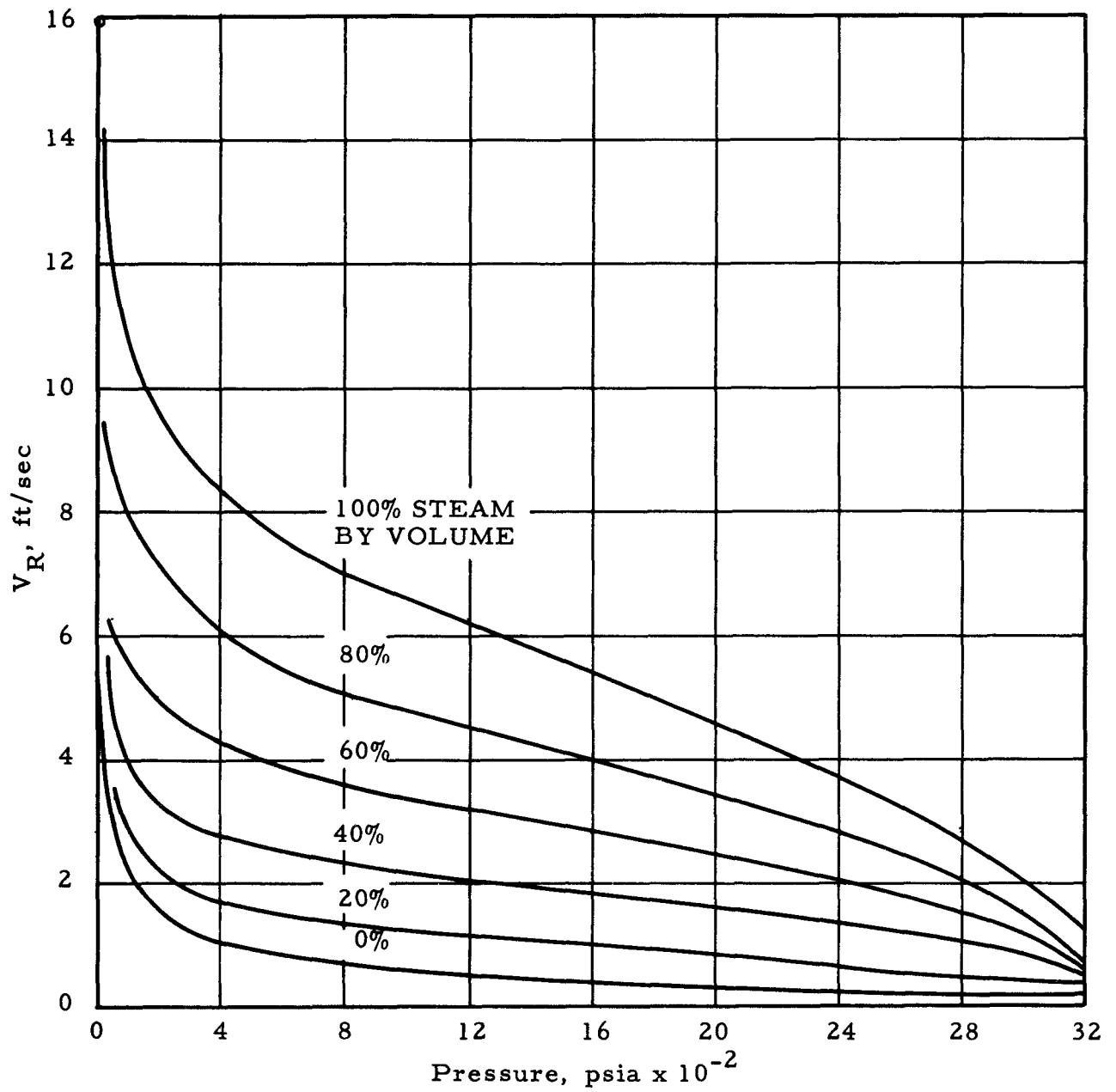
FIG. 2: COMPARISON OF CALCULATION METHOD WITH EXPERIMENTAL DATA
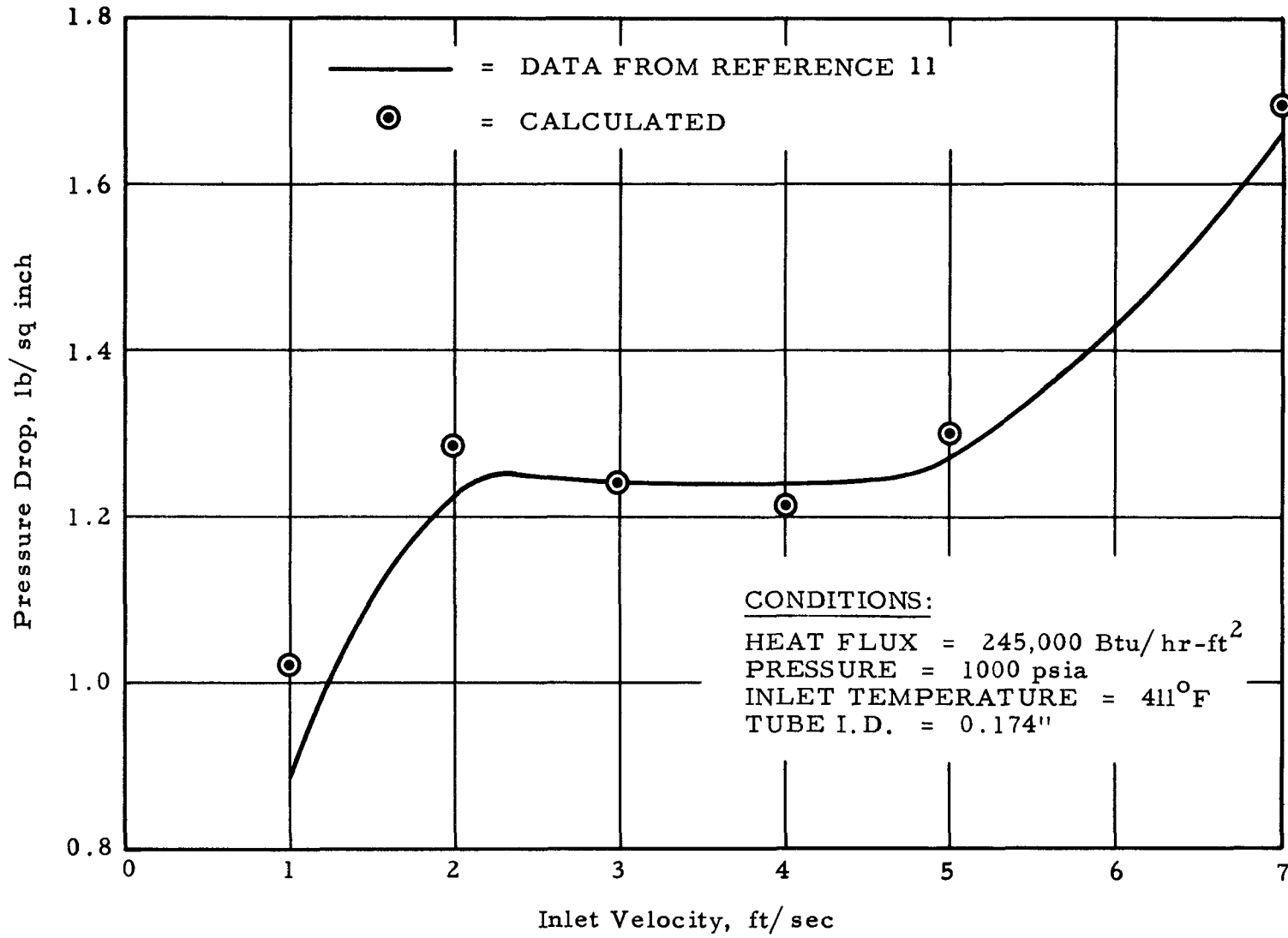
FIG. 3: CETR PRESSURE MAP
(Based on Fuel Element Flow Test)

Relative Pressure, psi
(excluding static head)

Position in Reactor

Identification of Flow Paths

O through fuel elements
□ between fuel elements
△ through control rod guide tubes

▲ through thermal shields
■ between core shroud and
inner thermal shield

⑤ denotes orifice location
● denotes mixing or separation
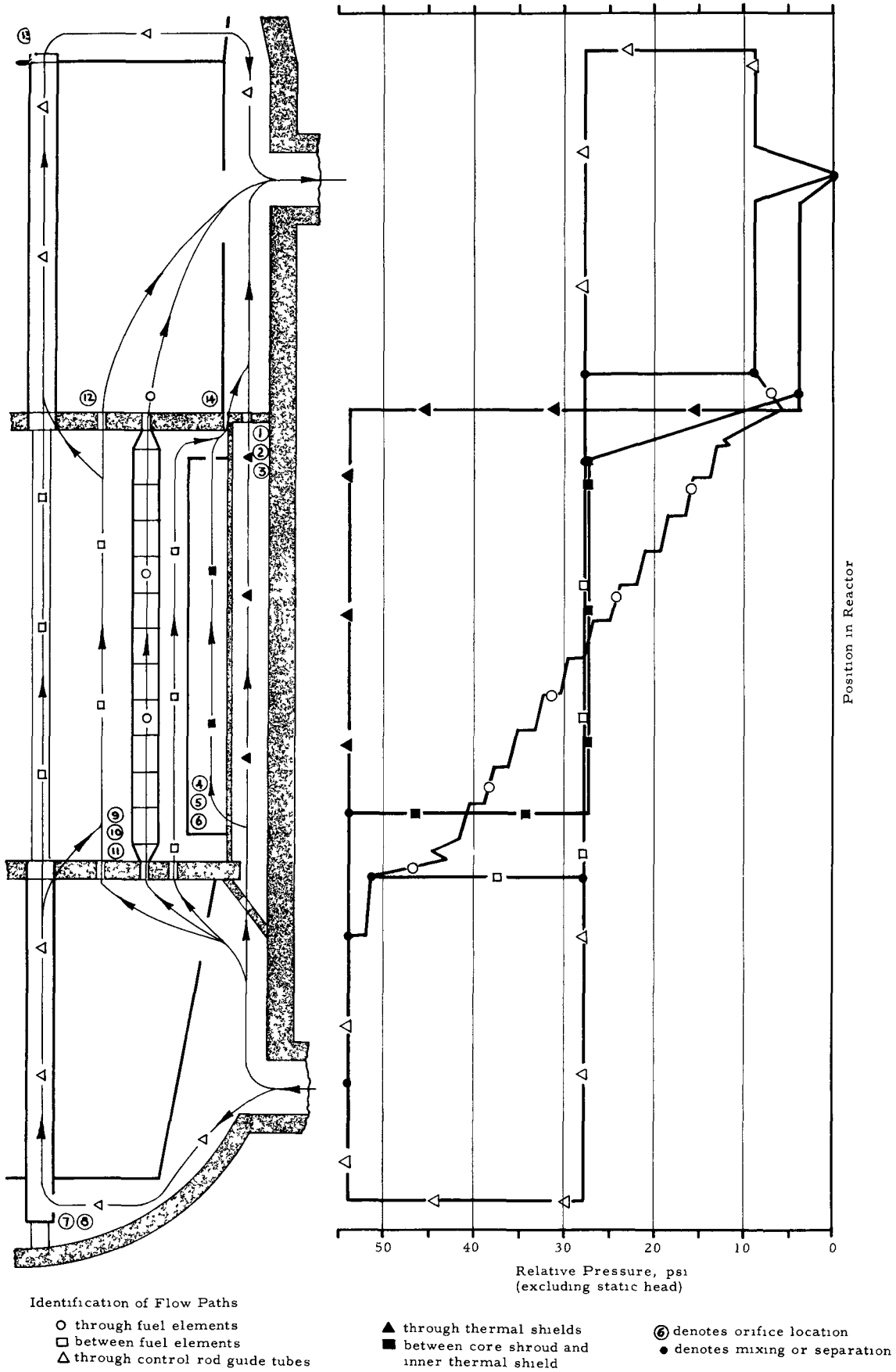
FIG. 4: ORIFICE LOCATIONS FOR CETR CORE
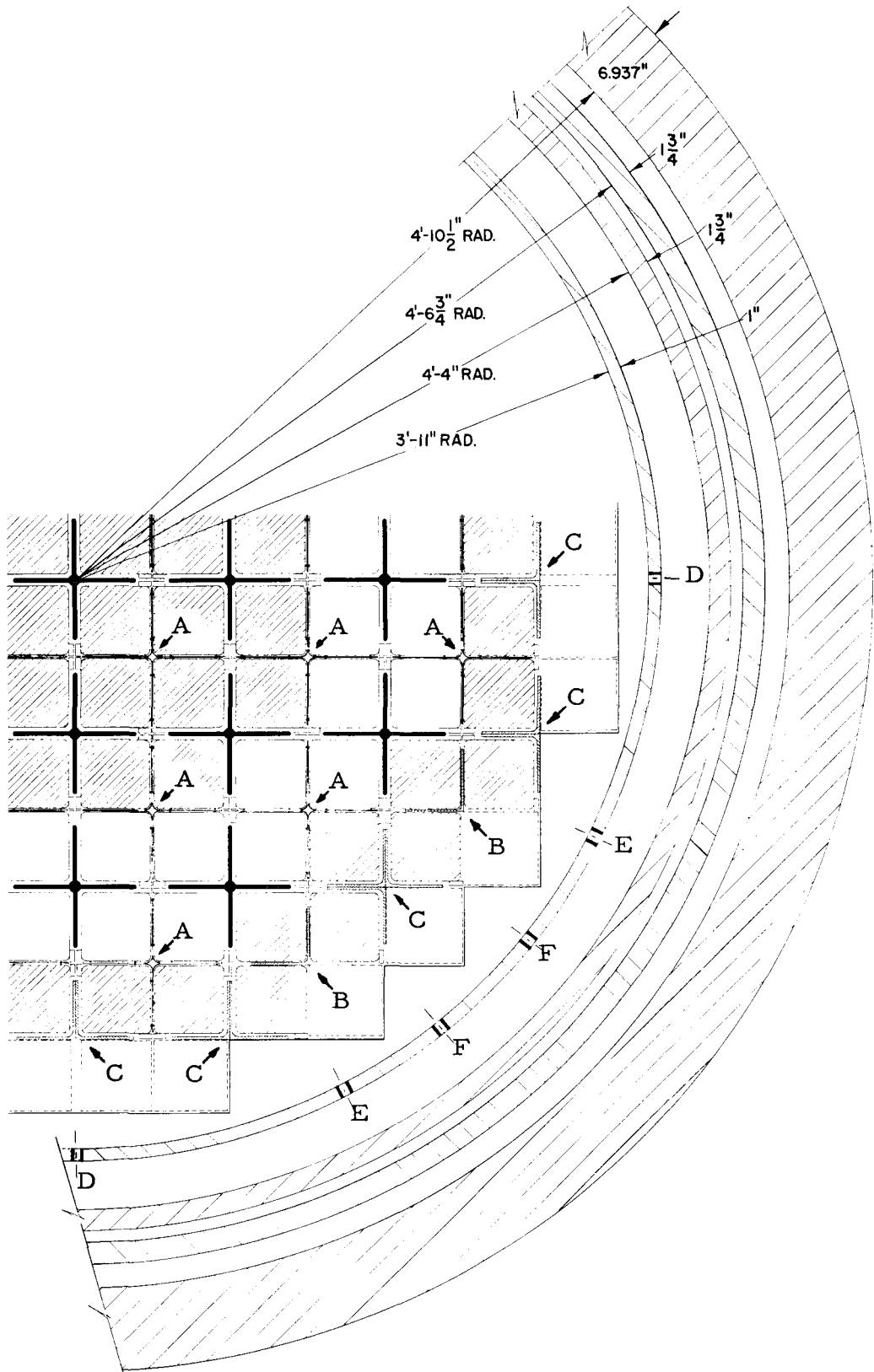
FIG. 5: COMPARISON OF BURNOUT CORRELATIONS

Legend
A - B&W Best Fit
B - Jens & Lottes Ref 23
C - WAPD Ref 26
D - B&W Max Permissible
E - B&W Max Design

Steam Quality = 0

Pressure = 1500 psia
$G = 10^6$ lb/hr/sq ft

Heat Flux, Btu/hr ft^2 F

10^6

10^5

400   500   600   700   800   900   1000

Enthalpy, BTU/lb
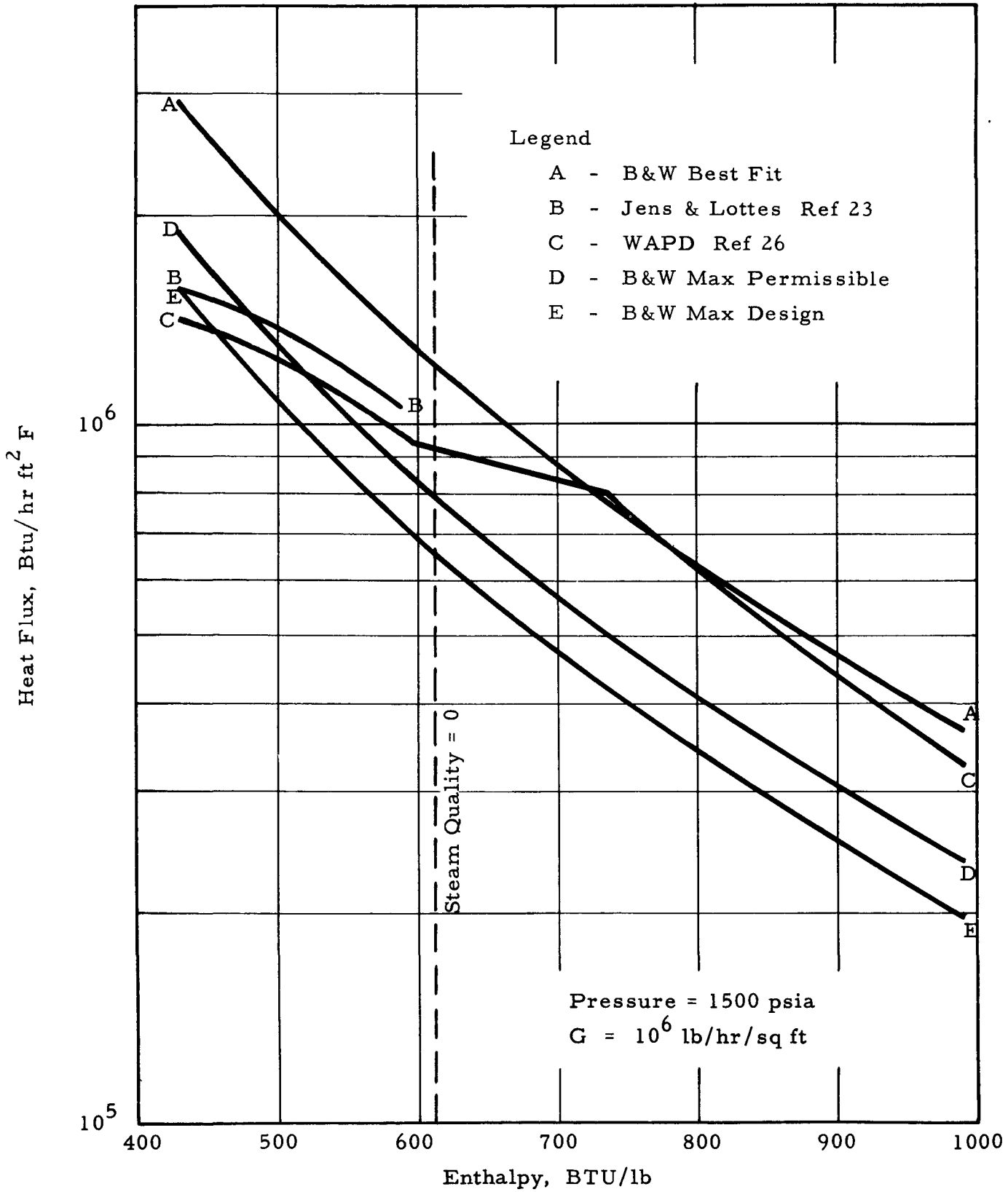
FIG. 6: BURNOUT ANALYSIS
(RATED POWER 585 MW)
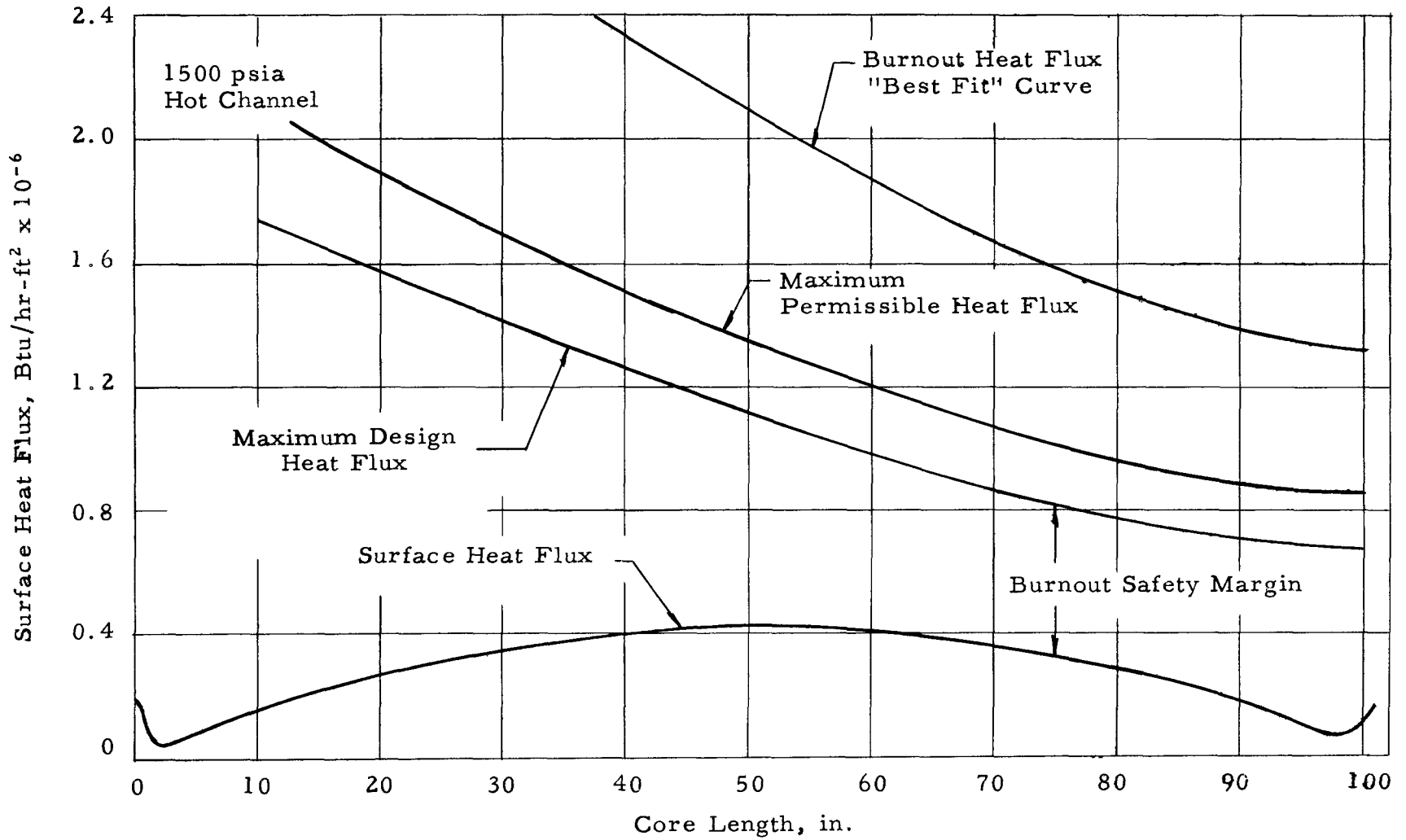
FIG. 7: BURNOUT ANALYSIS
(143% RATED POWER 837 MW)
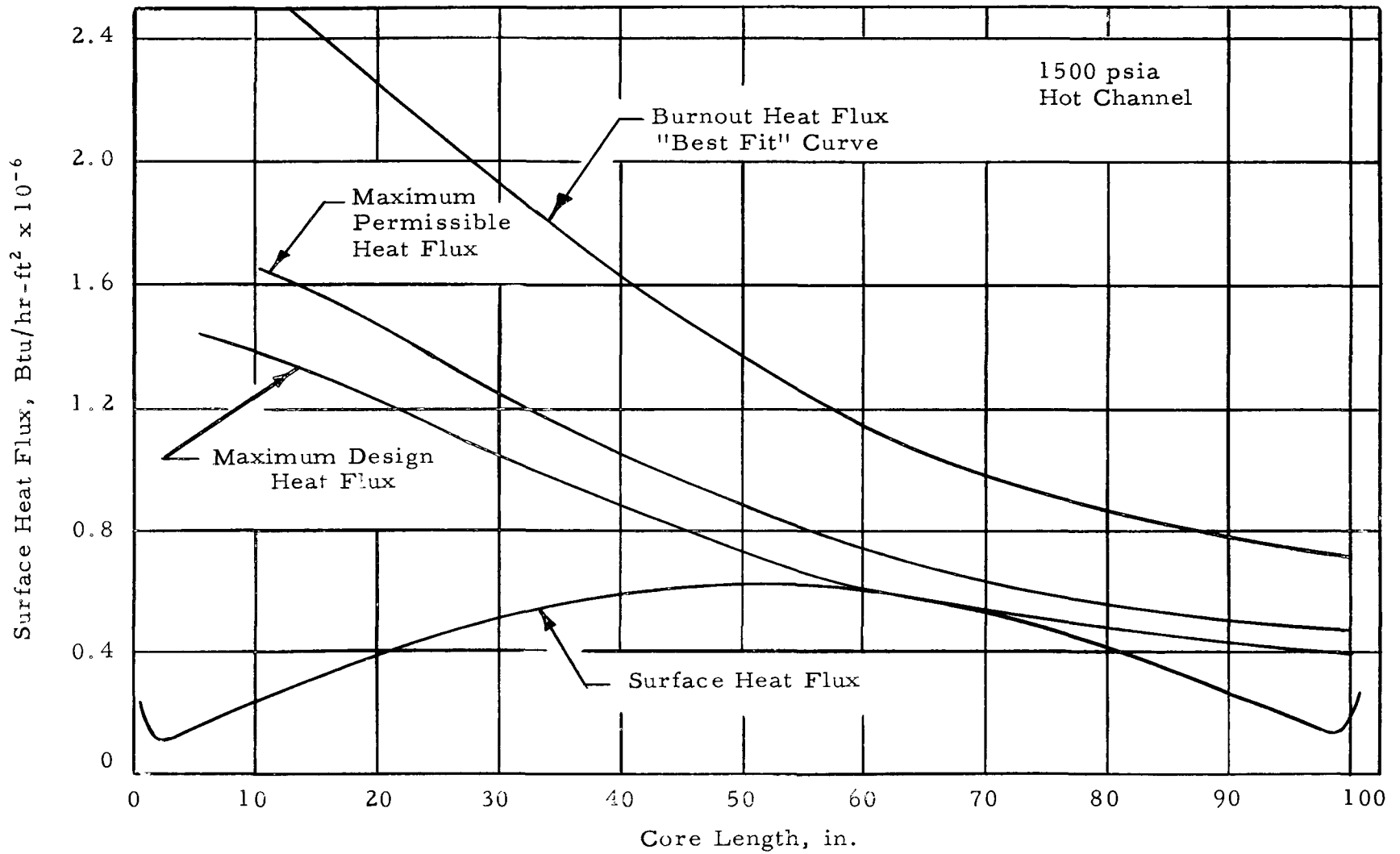
FIG. 8: FUEL CENTRAL TEMPERATURE CETR FUEL ELEMENT
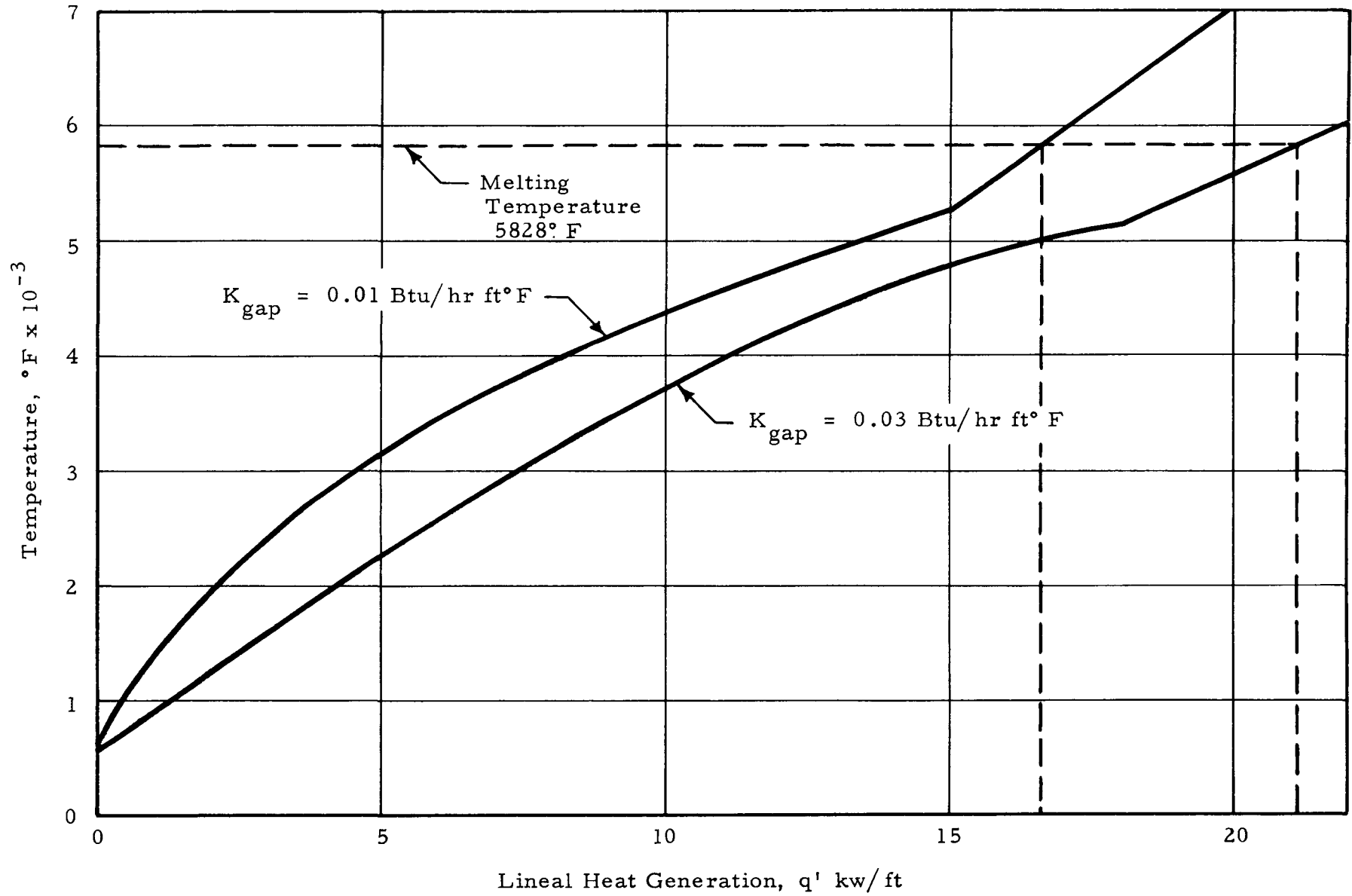
FIG. 9: EFFECT OF LOCAL BOILING ON CLAD SURFACE TEMPERATURE
632 MWH   108% RATED POWER
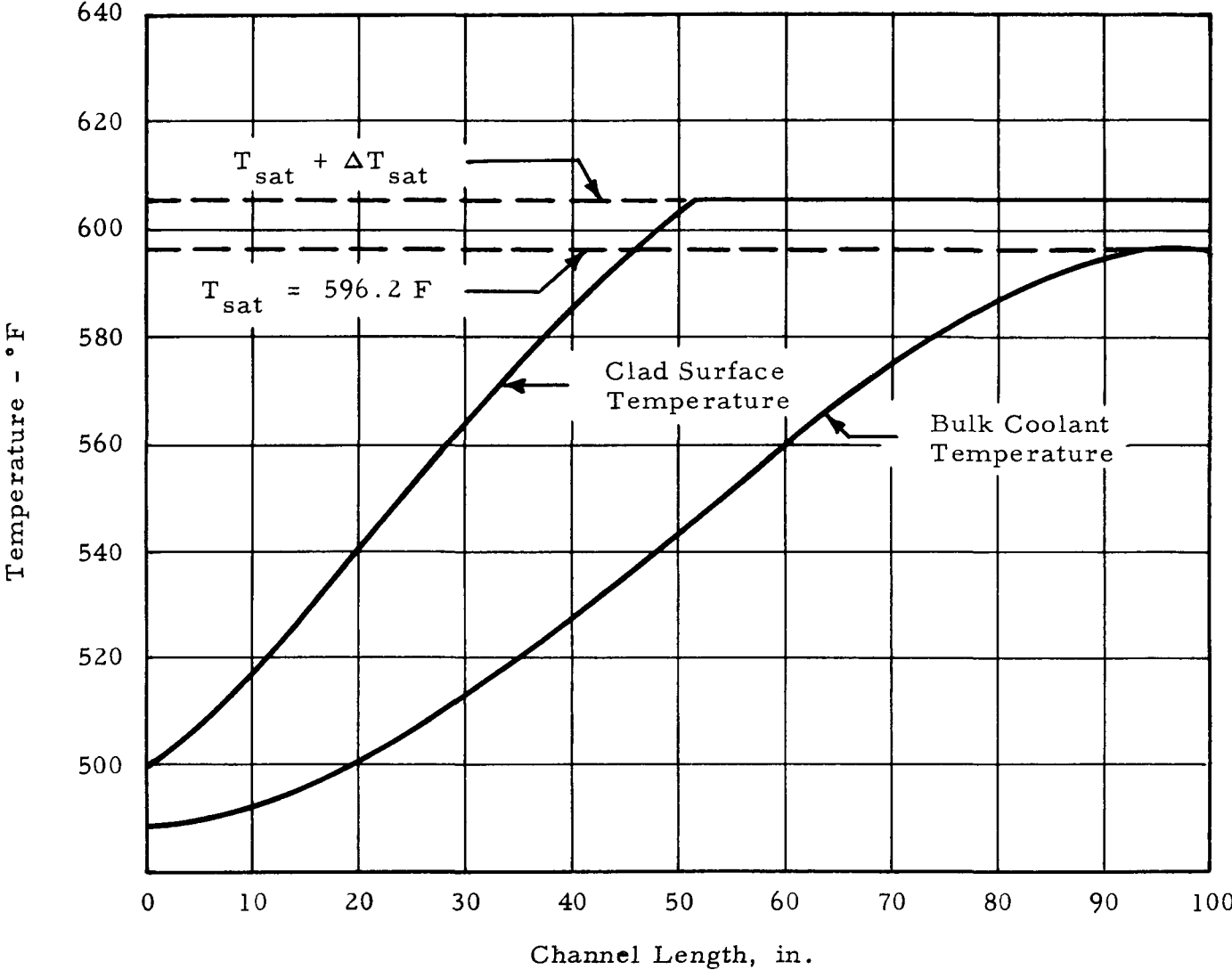
FIG. 10: PARTIAL LOSS OF FLOW
8 PUMPS TO 6 PUMPS IN 4 LOOPS

TOTAL REACTOR FLOW

NORMAL FLOW = 14, 972 lb/sec
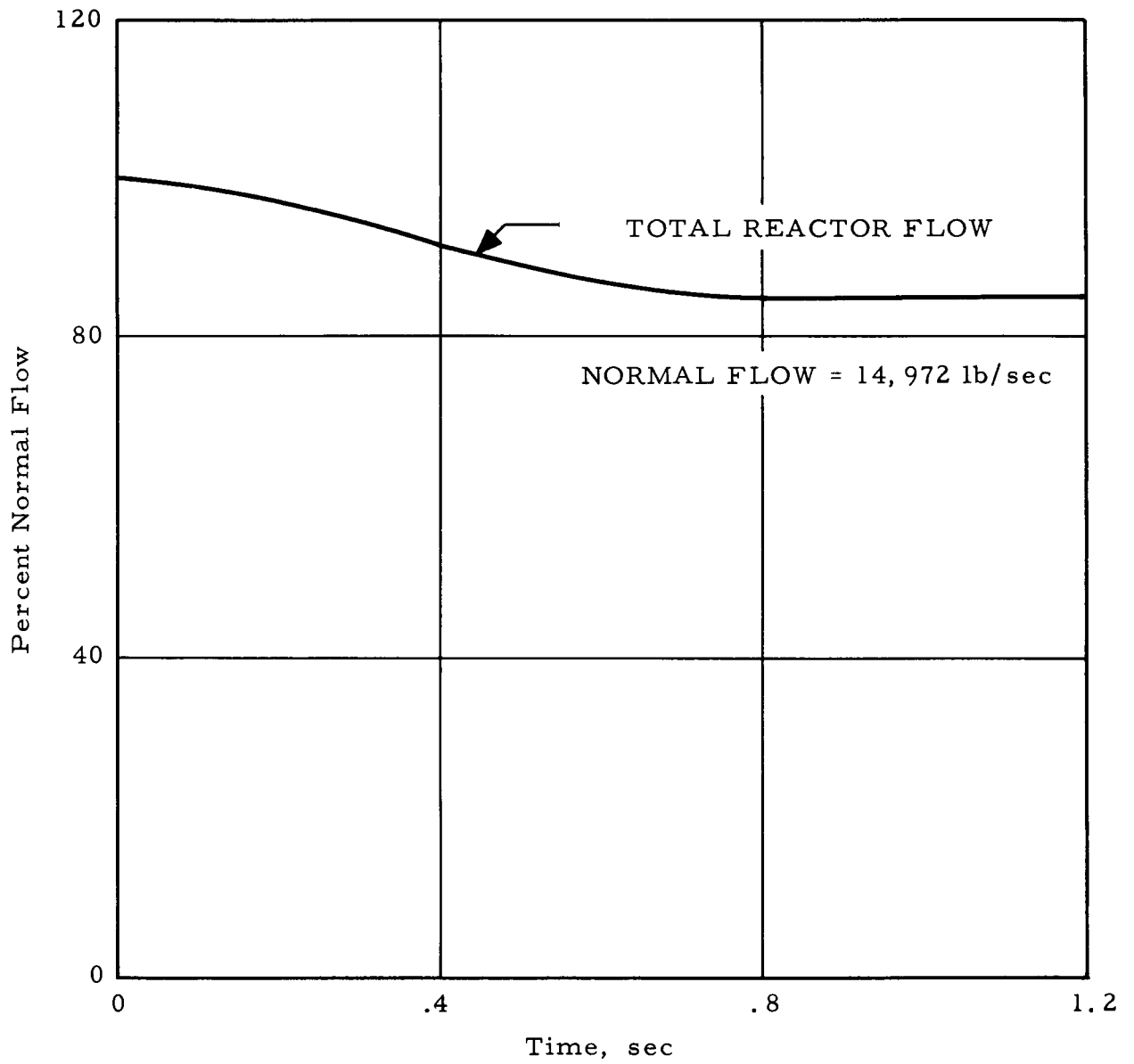
FIG. 11: PARTIAL LOSS OF FLOW
8 PUMPS TO 6 PUMPS IN 3 LOOPS
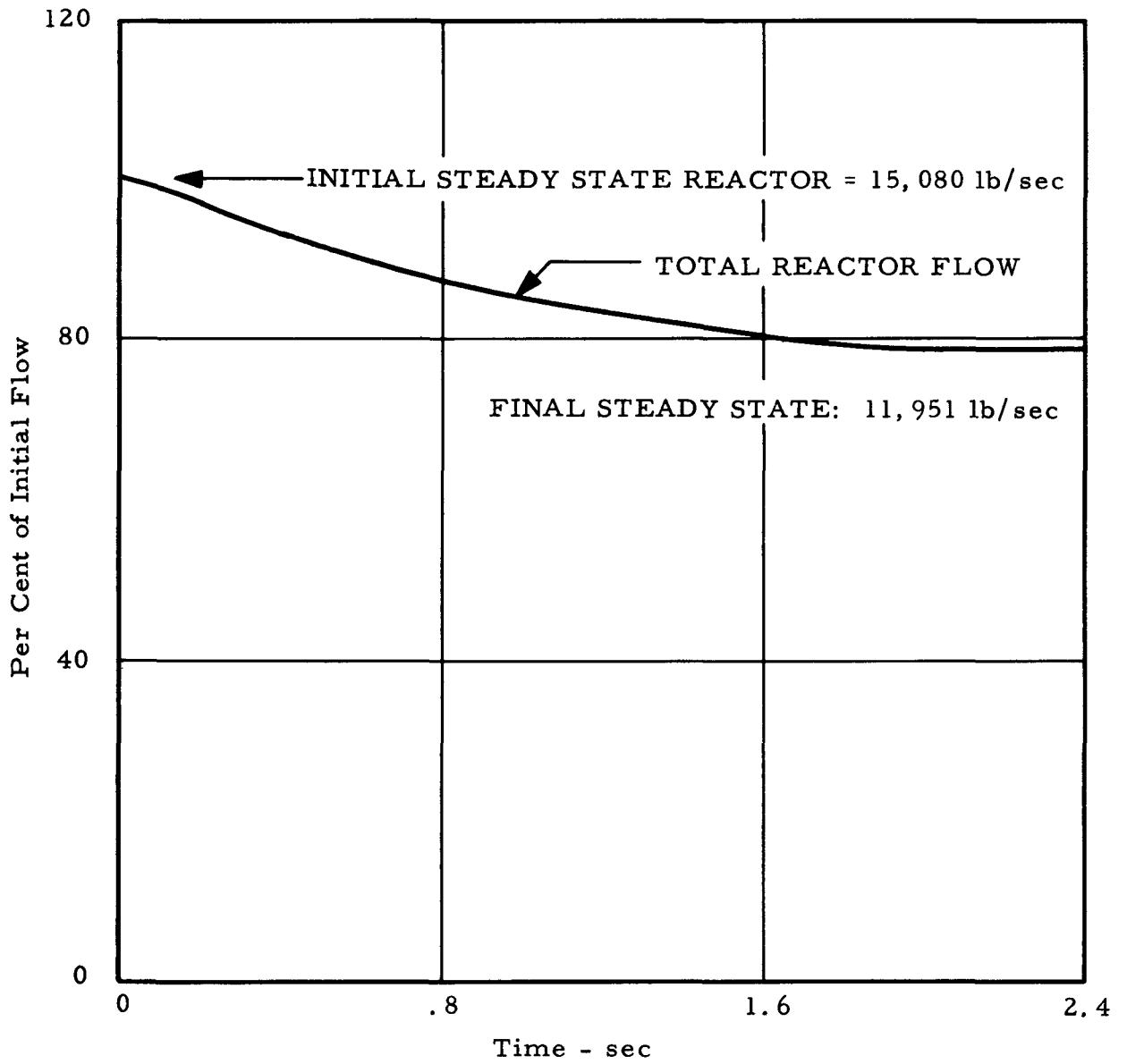
FIG. 12: FLOW COASTDOWN DUE TO LOSS OF PUMPING POWER

FIG. 13: FLOW COASTDOWN DUE TO LOSS OF PUMPING POWER

2- PUMPS OPERATING INITIALLY

Percent Normal Flow

Time, seconds
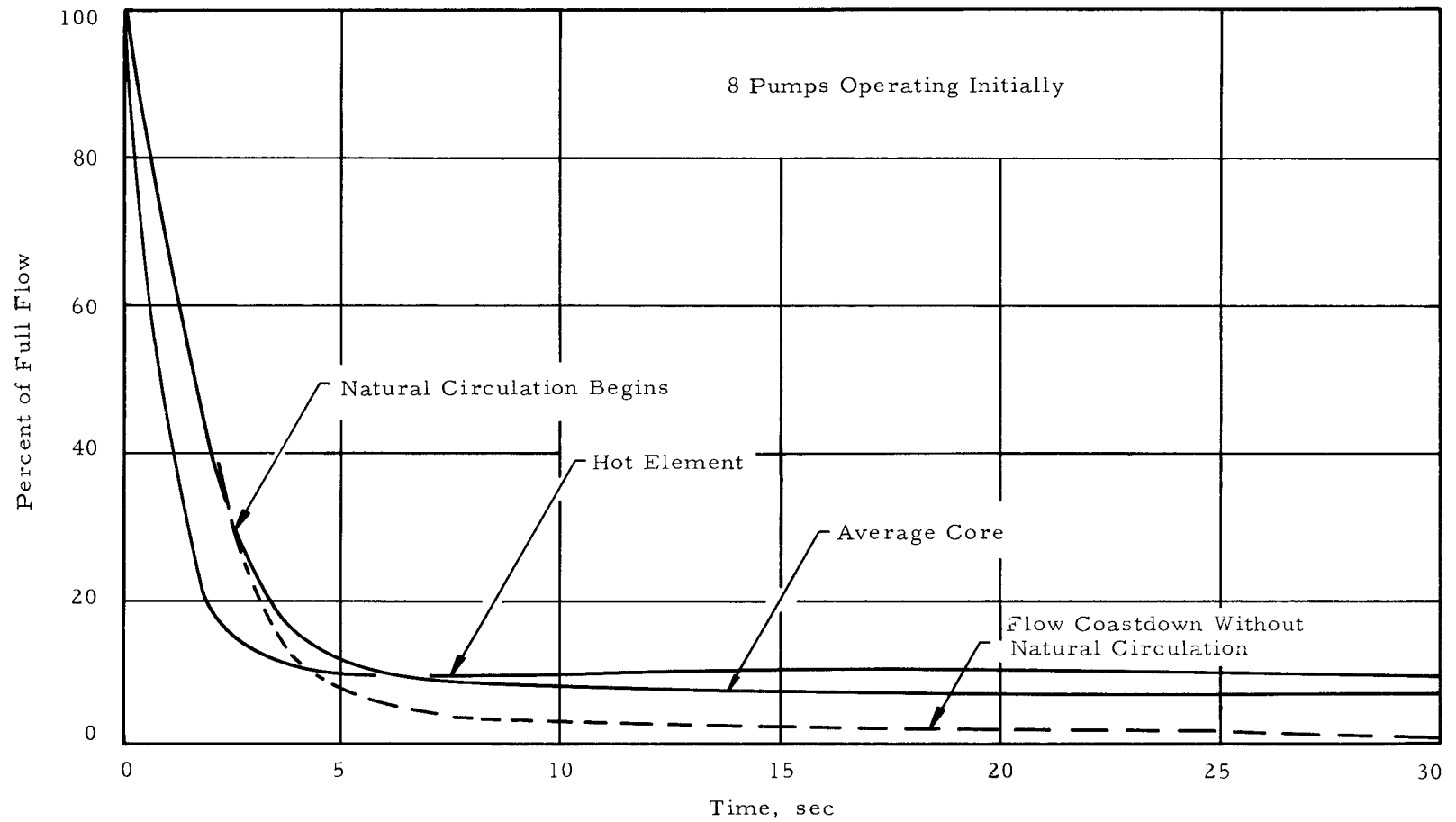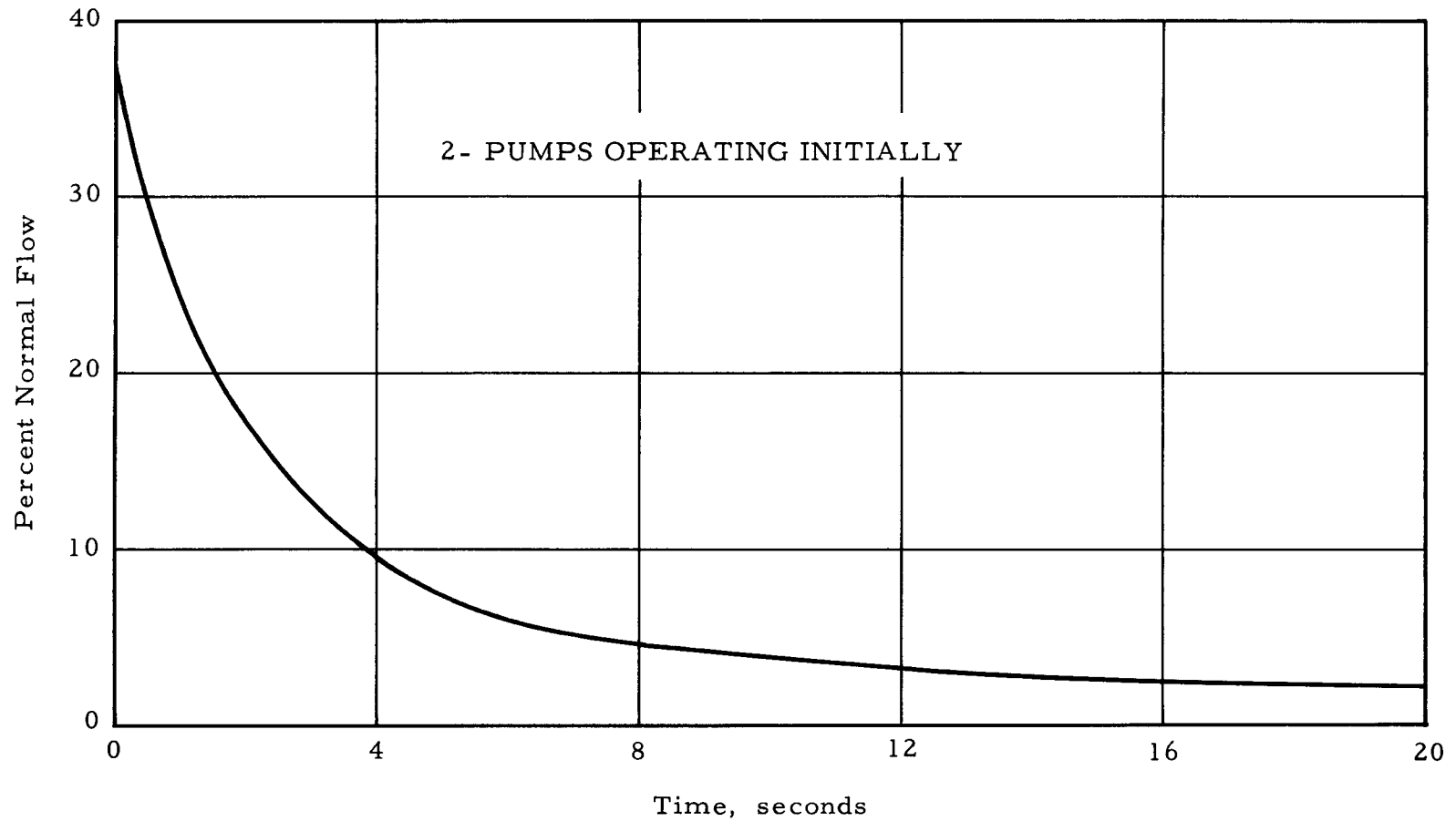
FIG. 14: POWER LEVEL DURING FLOW COASTDOWN
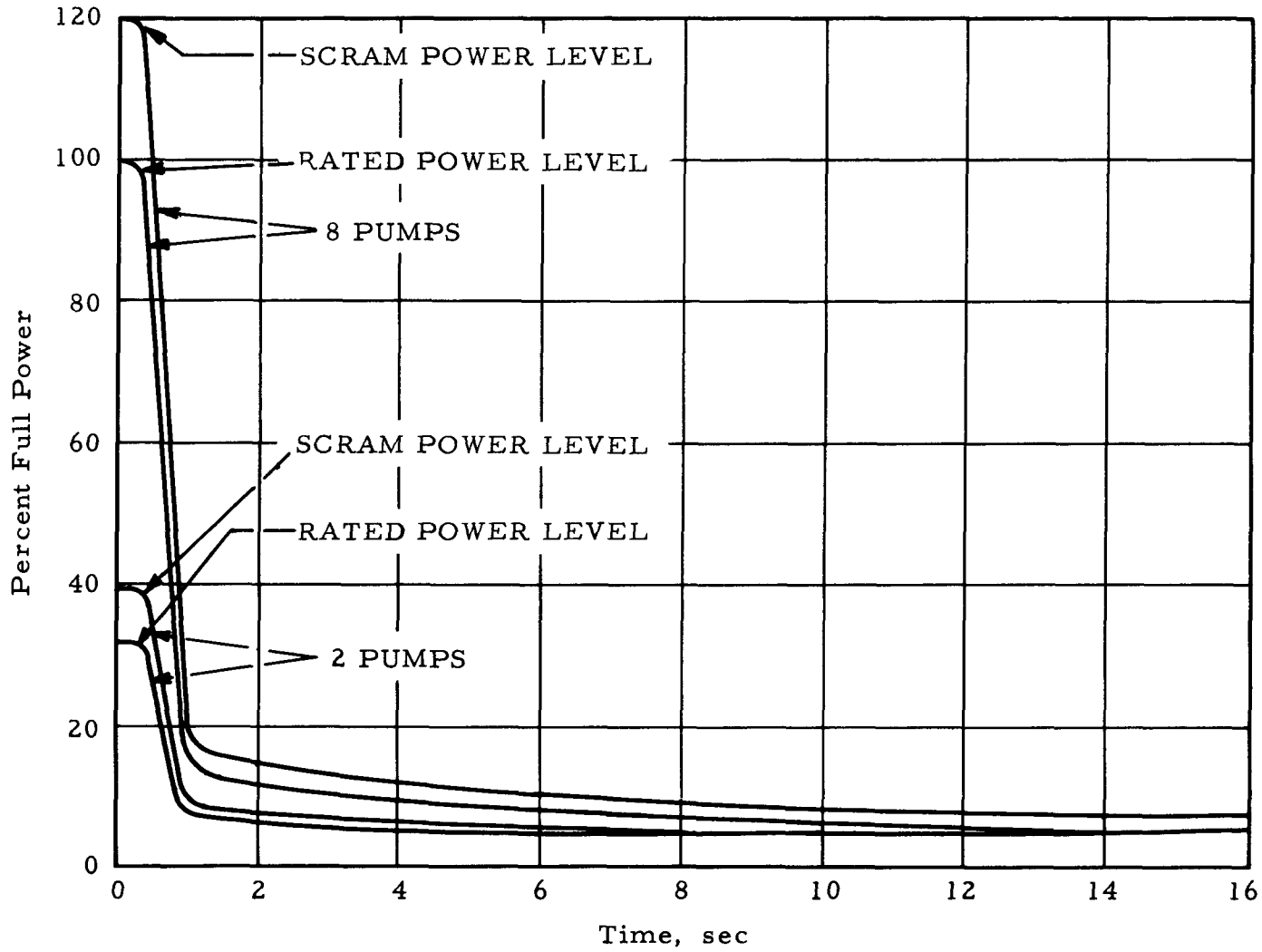
FIG. 15: LOSS OF FORCED COOLANT FLOW INCIDENT (100% RATED FLOW, 120% RATED POWER)
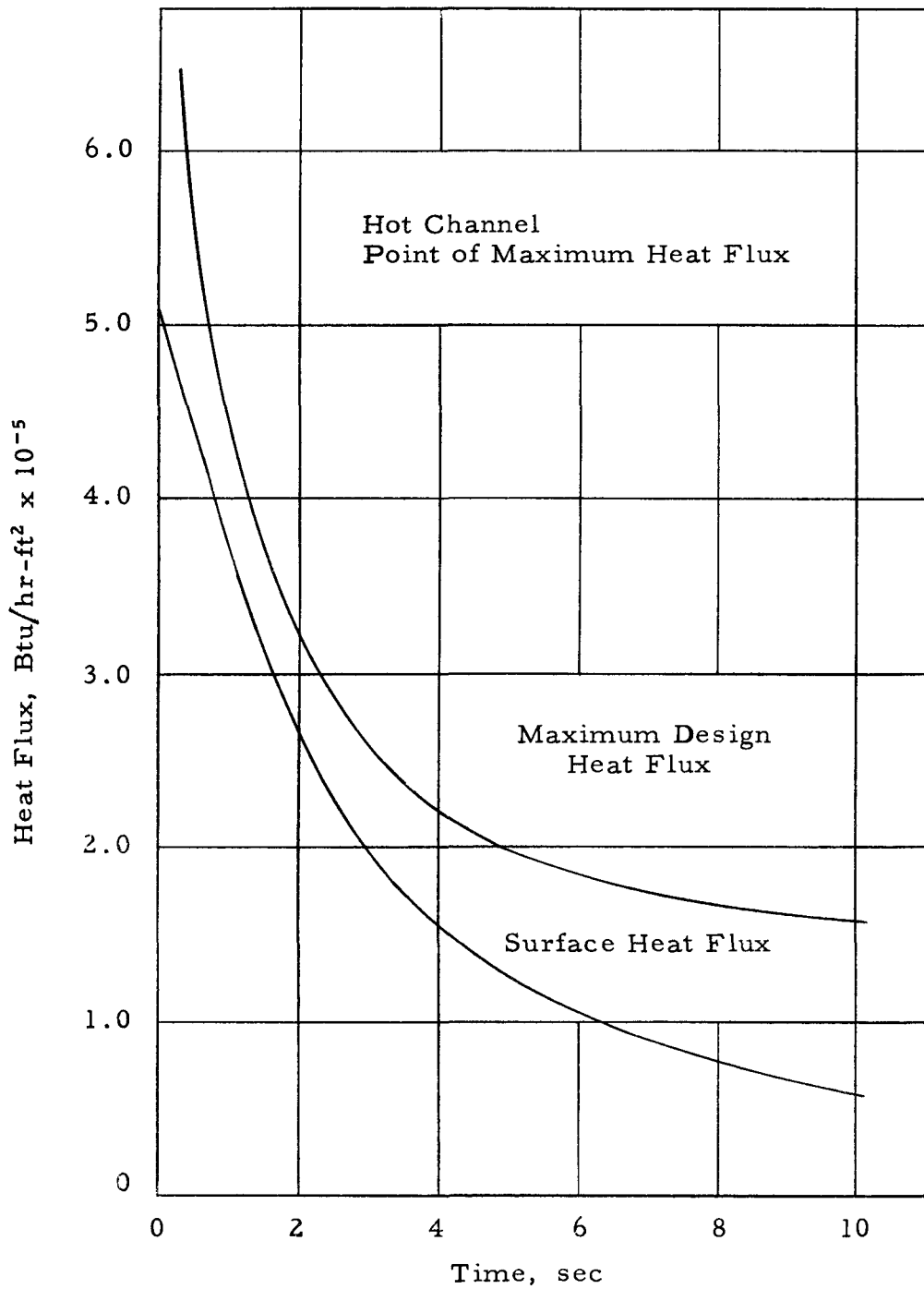
FIG. 16: LOSS OF FORCED COOLANT FLOW INCIDENT
(100% RATED FLOW, 100 % RATED POWER)
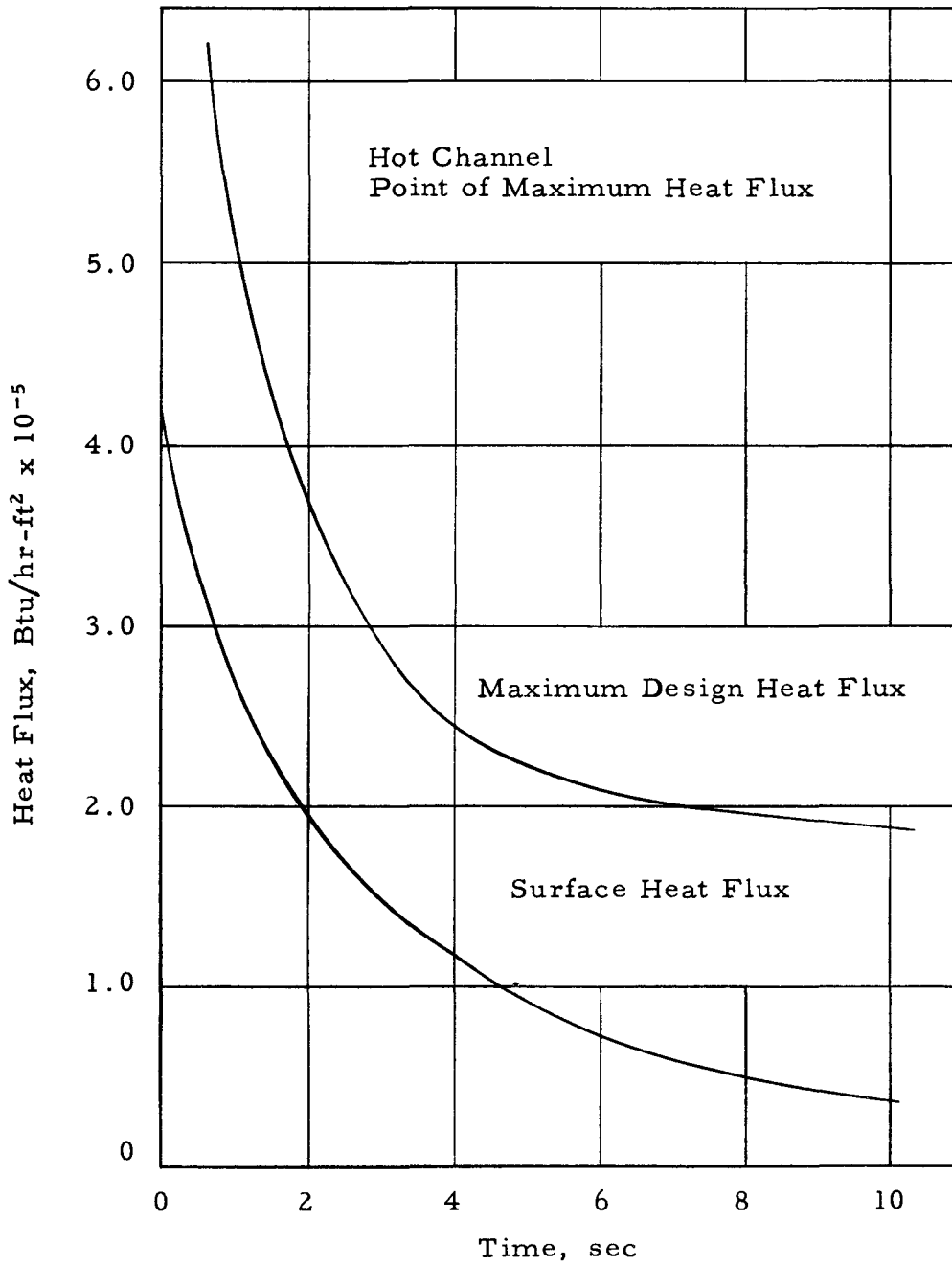
FIG. 17: LOSS OF FORCED COOLANT FLOW INCIDENT
(35.8% RATED FLOW, 39% RATED POWER)
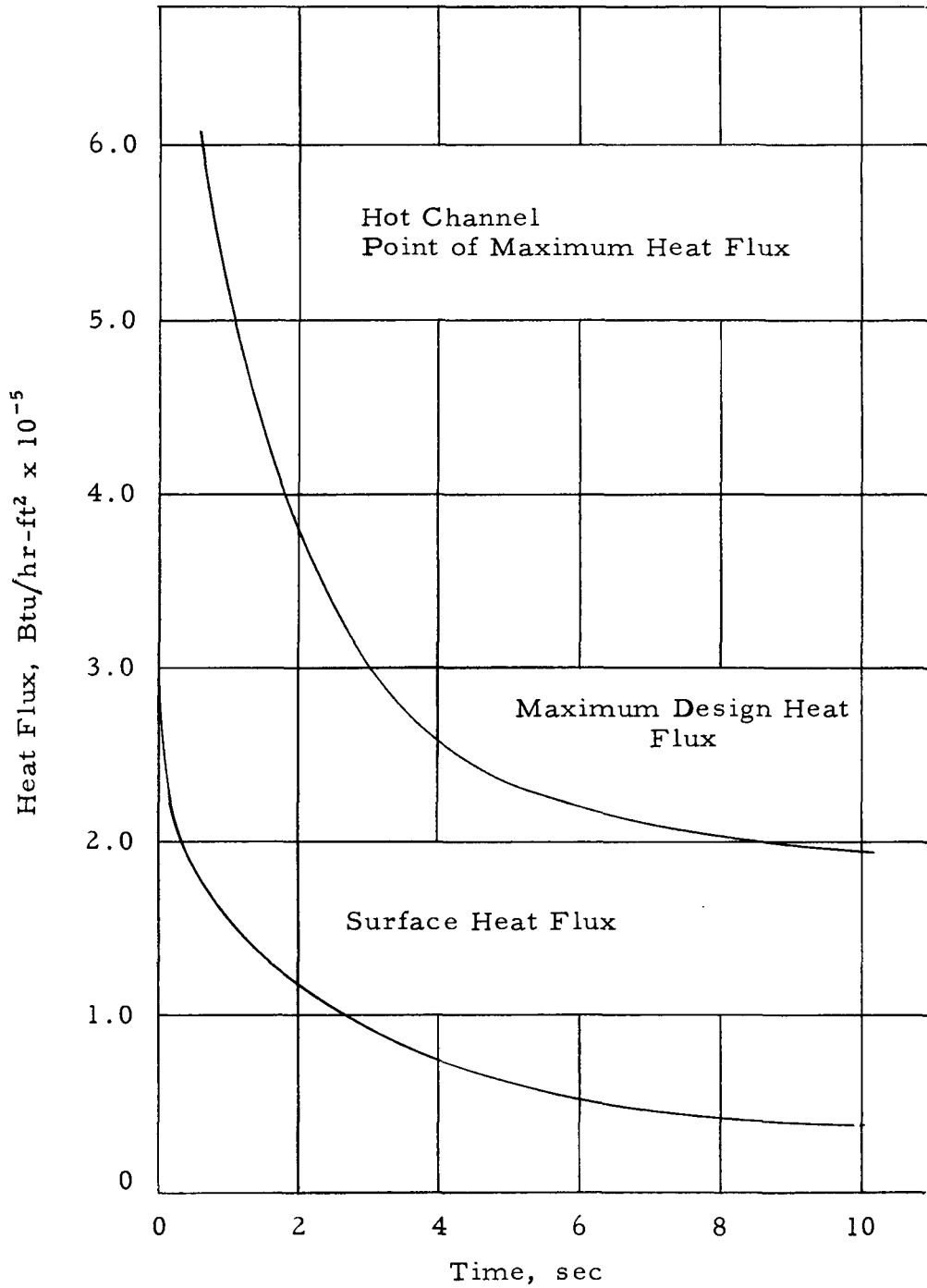
FIG. 18: LOSS OF FORCED COOLANT FLOW INCIDENT
(35.8% RATED FLOW, 32.5% RATED POWER)
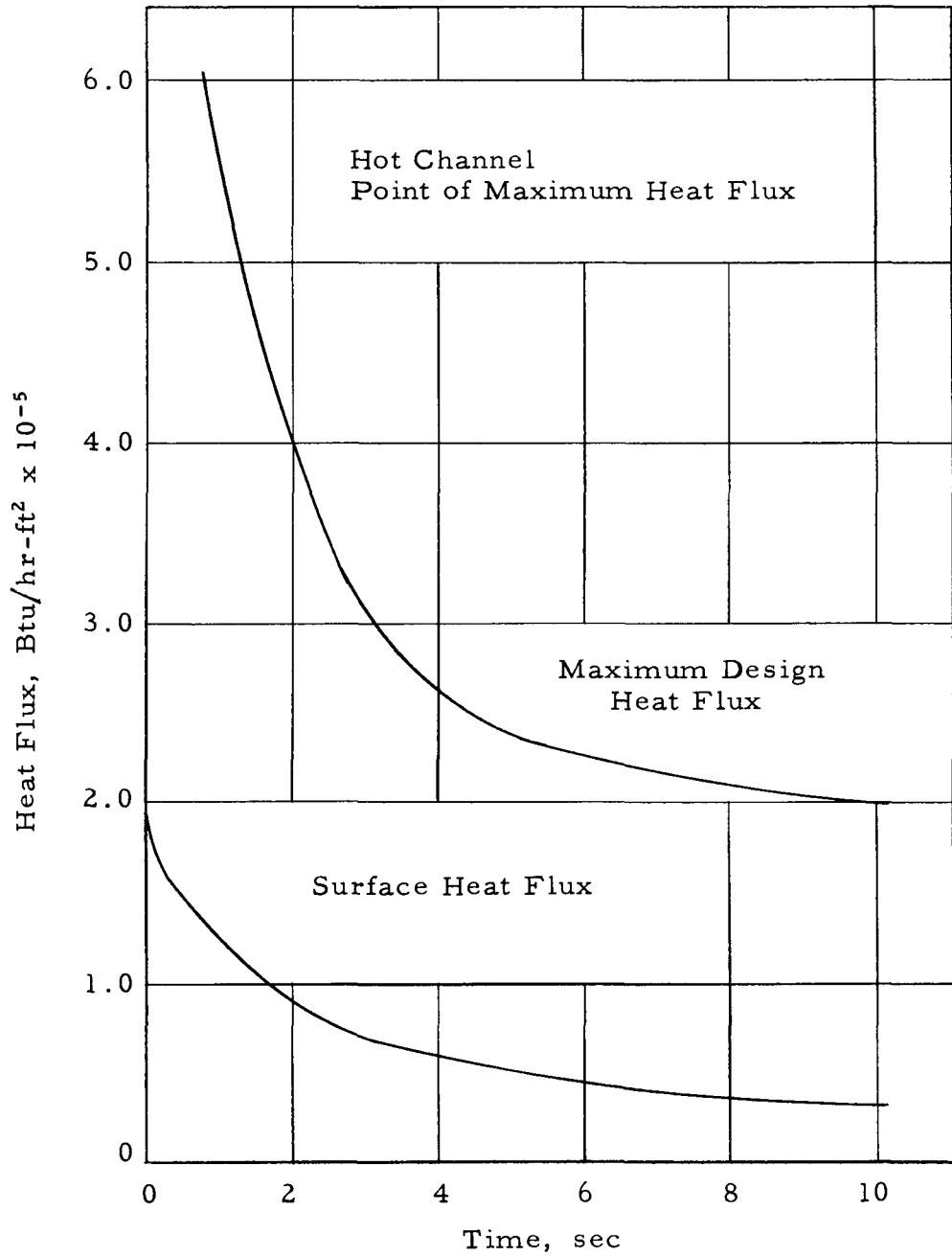
536-067

FIG. 19: LOSS OF FORCED COOLANT FLOW INCIDENT
(FUEL ELEMENT TEMPERATURE, 100% RATED FLOW)
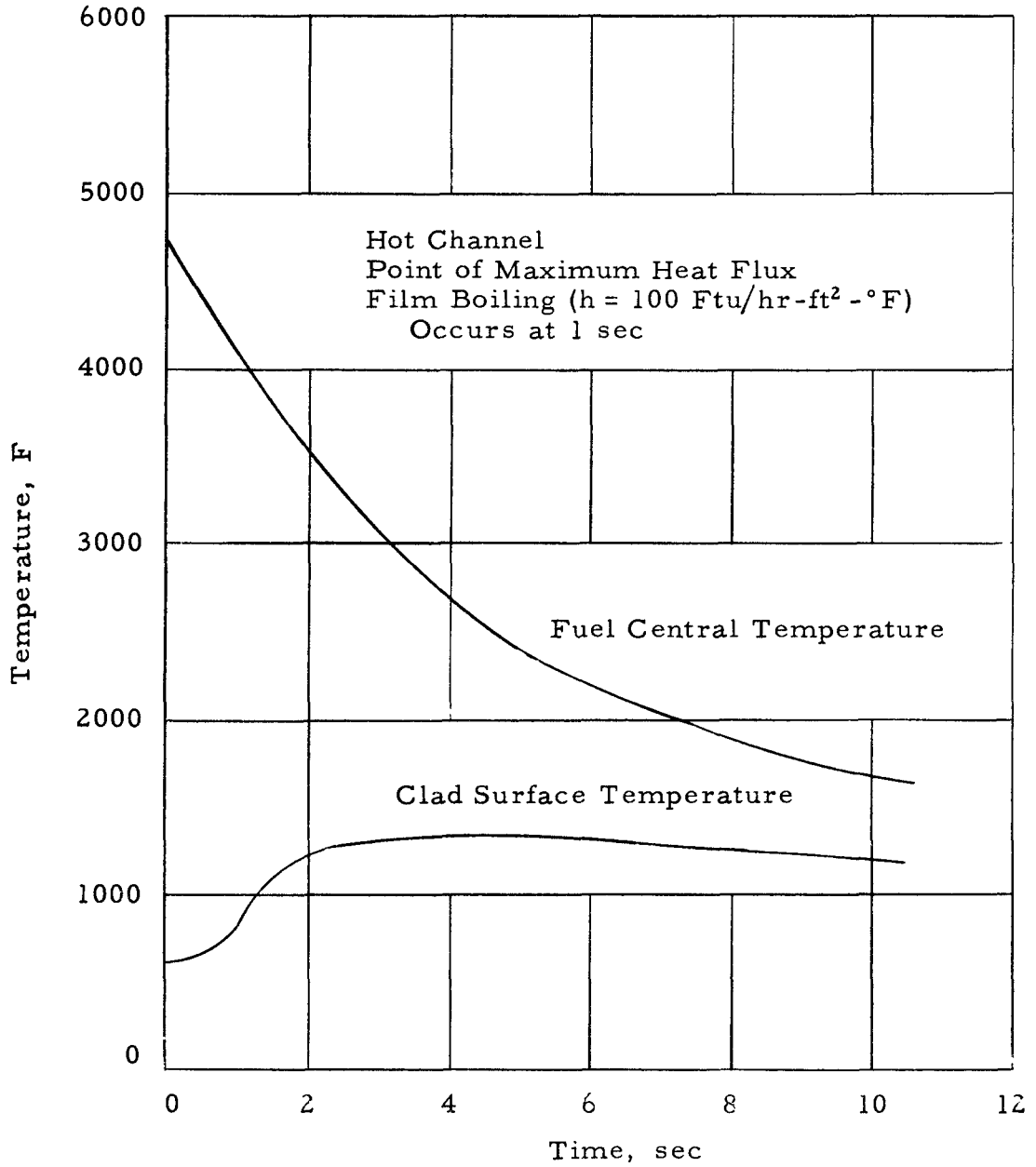
FIG. 20: LOSS OF FORCED COOLANT FLOW INCIDENT
(FUEL ELEMENT TEMPERATURE, 35.8% RATED FLOW)